LETTER

https://doi.org/10.1038/s41586-018-0392-8

Exosomal PD–L1 contributes to immunosuppression and is associated with anti–PD–1 response

Gang Chen[1], Alexander C. Huang[2], Wei Zhang[1,3], Gao Zhang[4], Min Wu[1], Wei Xu[5], Zili Yu[3], Jiegang Yang[1,3], Beike Wang[1,3], Honghong Sun[6], Houfu Xia[3], Qiwen Man[3], Wenqun Zhong[1,3], Leonardo F. Antelo[5], Bin Wu[1], Xuepeng Xiong[3], Xiaoming Liu[6], Lei Guan[1,7], Ting Li[6,7], Shujing Liu[6], Ruifeng Yang[6], Youtao Lu[1], Liyun Dong[6], Suzanne McGettigan[2], Rajasekharan Somasundaram[4], Ravi Radhakrishnan[8], Gordon Mills[9], Yiling Lu[9], Junhyong Kim[1], Youhai H. Chen[6], Haidong Dong[10], Yifang Zhao[3], Giorgos C. Karakousis[6], Tara C. Mitchell[2,5], Lynn M. Schuchter[2,5], Meenhard Herlyn[4], E. John Wherry[11,12], Xiaowei Xu[6]* & Wei Guo[1]*

Tumour cells evade immune surveillance by upregulating the surface expression of programmed death-ligand 1 (PD-L1), which interacts with programmed death-1 (PD-1) receptor on T cells to elicit the immune checkpoint response[1,2]. Anti-PD-1 antibodies have shown remarkable promise in treating tumours, including metastatic melanoma[2–4]. However, the patient response rate is low[4,5]. A better understanding of PD-L1-mediated immune evasion is needed to predict patient response and improve treatment efficacy. Here we report that metastatic melanomas release extracellular vesicles, mostly in the form of exosomes, that carry PD-L1 on their surface. Stimulation with interferon-γ (IFN-γ) increases the amount of PD-L1 on these vesicles, which suppresses the function of CD8 T cells and facilitates tumour growth. In patients with metastatic melanoma, the level of circulating exosomal PD-L1 positively correlates with that of IFN-γ, and varies during the course of anti-PD-1 therapy. The magnitudes of the increase in circulating exosomal PD-L1 during early stages of treatment, as an indicator of the adaptive response of the tumour cells to T cell reinvigoration, stratifies clinical responders from non-responders. Our study unveils a mechanism by which tumour cells systemically suppress the immune system, and provides a rationale for the application of exosomal PD-L1 as a predictor for anti-PD-1 therapy.

Extracellular vesicles, such as exosomes and microvesicles (also known as shedding vesicles), carry bioactive molecules that influence the extracellular environment and the immune system[6–8]. We purified exosomes from a panel of human primary and metastatic melanoma cell lines by differential centrifugation[9–12], and verified them by transmission electron microscopy (TEM) and nanoparticle tracking analysis (NTA) (Fig. 1a, b). Proteins associated with the exosomes were then analysed by reverse phase protein array (RPPA), a large-scale antibody-based quantitative proteomics technology[13]. Analysis by RPPA and western blot revealed the presence of PD-L1 in exosomes, and its level was significantly higher in exosomes derived from metastatic melanoma cells compared to those from primary melanoma cells (Fig. 1c, d, Extended Data Fig. 1a). Iodixanol density gradient centrifugation further confirmed the association of PD-L1 with the exosomes (Extended Data Fig. 1b). PD-L1 was also detected in microvesicles, but at a lower level (Extended Data Fig. 1c–e). PD-L1 was also detected in extracellular vesicles generated from mouse metastatic melanoma B16-F10 cells (Extended Data Fig. 1f).

Tumour cell surface PD-L1 can be upregulated in response to IFN-γ secreted by activated T cells, and PD-L1 binds to PD-1 through its extracellular domain to inactivate T cells[2,3,14]. Using immuno-electron microscopy and enzyme-linked immunosorbent assay (ELISA) (Fig. 1e–g), we found that exosomal PD-L1 has the same membrane topology as cell surface PD-L1, with its extracellular domain exposed on the surface of the exosomes. Exosomal PD-L1 binds PD-1 in a concentration-dependent manner, and this interaction can be disrupted by PD-L1-blocking antibodies (Fig. 1h). Furthermore, the level of exosomal PD-L1 secreted by melanoma cells increased markedly upon IFN-γ treatment (Fig. 1f, g, i), and correspondingly, these exosomes displayed increased binding to PD-1 (Fig. 1h).

Exosomes are generated and released through a defined intracellular trafficking route[7,9,10]. Genetic knockdown of the ESCRT subunit Hrs, which mediates the recognition and sorting of exosomal cargos[15], using short hairpin (sh)RNA led to a decrease in the level of PD-L1 in the exosomes and an increase of PD-L1 in the cell (Extended Data Fig. 1g, h). In addition, PD-L1 co-immunoprecipitated with Hrs from cell lysates (Extended Data Fig. 1i). PD-L1 co-localized with Hrs and CD63, an exosome marker, in melanoma cells (Extended Data Fig. 1j, k). Knockdown of Rab27A, which mediates exosome release[16], also blocked PD-L1 secretion via the exosomes (Extended Data Fig. 1l).

To investigate the secretion of exosomal PD-L1 by melanoma cells in vivo, we established human melanoma xenografts in nude mice. Blood from these mice was collected for exosome purification and subsequent detection of human PD-L1 proteins by ELISA (Fig. 2a). Antibodies against human PD-L1 specifically identified human PD-L1 on the circulating exosomes from mice bearing human melanoma xenografts but not the control mice (Fig. 2b, Extended Data Fig. 2a, b). Moreover, the level of circulating exosomal PD-L1 positively correlated with tumour size (Fig. 2c).

PD-L1 has been found in blood samples derived from melanoma patients[17]. Recent studies suggest the presence of PD-L1 in extracellular vesicles isolated from blood samples of patients with cancer, and the level of PD-L1 correlates with pathological features of these patients[18–20]. We purified extracellular vesicles from the plasma of melanoma patients (Extended Data Fig. 2c–g). The level of PD-L1 on the circulating exosomes was significantly higher in patients with metastatic melanoma than in healthy donors (Fig. 2d, Extended Data Figs. 2f, 3a, 3b), whereas there was no or only marginal difference in the number of circulating exosomes or the total protein level on these exosomes (Extended Data Fig. 3c, d). There was less difference in PD-L1 levels in circulating microvesicles compared to the circulating exosomes (Extended Data Fig. 3e). The data analysis and receiver operating characteristic (ROC) curve show that, among all the parameters tested,

[1]Department of Biology, School of Arts & Sciences, University of Pennsylvania, Philadelphia, PA, USA. [2]Department of Medicine, Perelman School of Medicine, University of Pennsylvania, Philadelphia, PA, USA. [3]Key Laboratory of Oral Biomedicine Ministry of Education, School and Hospital of Stomatology, Wuhan University, Wuhan, China. [4]Molecular and Cellular Oncogenesis Program and Melanoma Research Center, The Wistar Institute, Philadelphia, PA, USA. [5]Abramson Cancer Center, Perelman School of Medicine, University of Pennsylvania, Philadelphia, PA, USA. [6]Department of Pathology and Laboratory Medicine, Perelman School of Medicine, University of Pennsylvania, Philadelphia, PA, USA. [7]Ministry of Education Key Laboratory of Biomedical Information Engineering, School of Life Science, Xi'an Jiaotong University, Xi'an, China. [8]Department of Bioengineering, School of Engineering, University of Pennsylvania, Philadelphia, PA, USA. [9]Department of Systems Biology, The University of Texas MD Anderson Cancer Center, Houston, TX, USA. [10]Department of Immunology, College of Medicine, Mayo Clinic, Rochester, MN, USA. [11]Institute for Immunology, Perelman School of Medicine, University of Pennsylvania, Philadelphia, PA, USA. [12]Department of Microbiology, Perelman School of Medicine, University of Pennsylvania, Philadelphia, PA, USA. *e-mail: xug@pennmedicine.upenn.edu; guowei@sas.upenn.edu

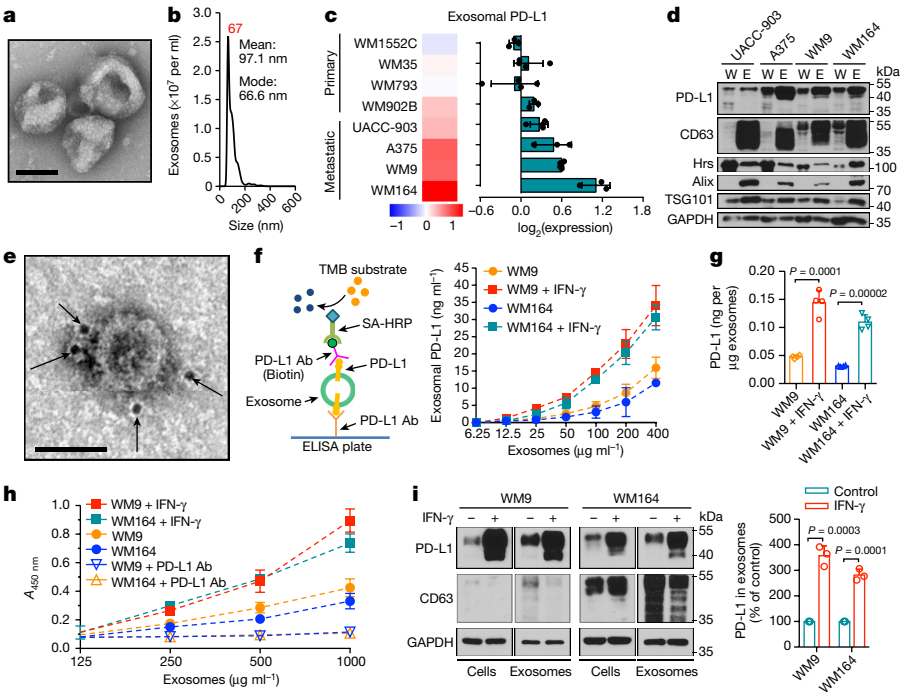

Fig. 1 | Extrafacial expression of PD-L1 on melanoma cell-derived exosomes and its regulation by IFN-γ. a, A representative TEM image of purified exosomes from WM9 cells. Scale bar, 50 nm. **b**, Characterization of purified exosomes using nanoparticle tracking. **c**, RPPA data showing the levels of PD-L1 in exosomes secreted by primary or metastatic melanoma cell lines ($n = 3$ for WM1552C, WM902B, A375, WM164; $n = 4$ for WM35, WM793, UACC-903, WM9). See Extended Data Fig. 1a for statistical analysis. **d**, Immunoblots for PD-L1 in the whole cell lysate (W) and purified exosomes (E) from different metastatic melanoma cell lines. All lanes were loaded with the same amount of total protein. **e**, A representative TEM image of WM9 cell-derived exosomes immunogold-labelled with anti-PD-L1 antibodies. Arrowheads indicate 5-nm gold particles. Scale bar, 50 nm. **f**, Schematic (left) of ELISA to measure PD-L1 concentration (right) on the surface of exosomes isolated from indicated cell types. TMB, 3, 3′, 5, 5′-tetramethylbenzidine; SA-HRP, streptavidin–horseradish peroxidase. **g**, ELISA of PD-L1 on exosomes from melanoma cells, with or without IFN-γ treatment. **h**, PD-l binding of exosomes with IFN-γ or blocking PD-L1 antibody (PD-L1 Ab) (see Methods). **i**, Western blot analysis of PD-L1 in whole cells and exosomes from IFN-γ-treated cells and control cells. All lanes were loaded with the same amount of total protein (left). Quantification of exosomal PD-L1 by western blotting (right). Results shown represent three (**a**, **b**) or two (**d**, **e**) independent experiments. Data are mean ± s.d. of three (**f**, **h**, **i**) or four (**g**) independent biological replicates. *P* values are from a two-sided unpaired *t*-test (**g**, **i**). Full gel source data (**d**, **i**) are shown in Supplementary Fig. 1.

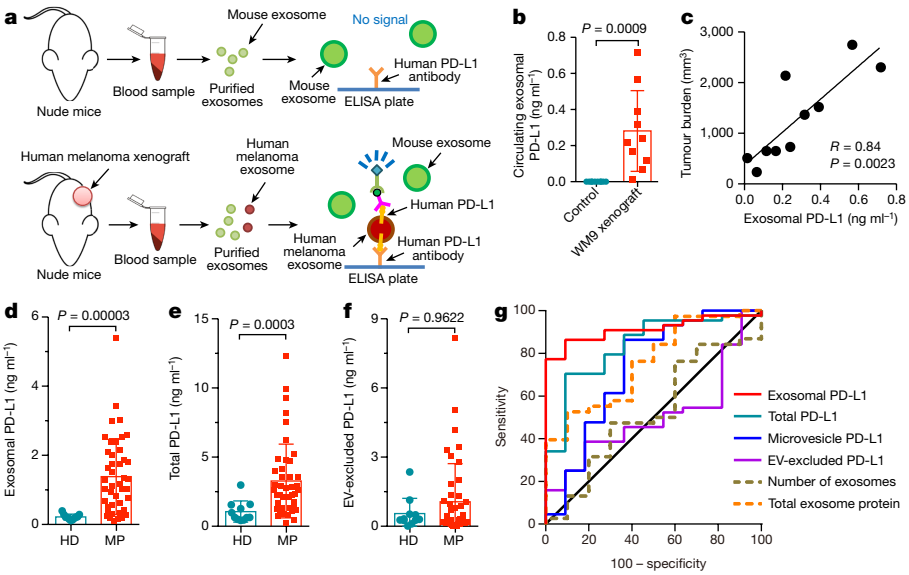

Fig. 2 | The level of PD-L1 on circulating exosomes distinguishes patients with metastatic melanoma from healthy donors. a, ELISA of human PD-L1 on exosomes in plasma samples from mice with human melanoma xenograft. **b**, Levels of PD-L1 on exosomes isolated from the plasma samples of control nude mice or mice bearing human WM9 melanoma xenograft, measured by ELISA ($n = 10$). **c**, Pearson correlation between the exosomal PD-L1 in plasma and tumour burden in xenograft-bearing nude mice ($n = 10$). **d**–**f**, ELISA of circulating exosomal PD-L1 (**d**), total PD-L1 (**e**) or extracellular vesicle (EV)-excluded PD-L1 (**f**) in healthy donors (HD, $n = 11$) and melanoma patients (MP, $n = 44$). The exosomes were purified using the exosome isolation kit. **g**, ROC curve analysis for the indicated parameters in patients with metastatic melanoma compared to healthy donors. Data are mean ± s.d. *P* values are from a two-sided unpaired *t*-test (**b**, **d**–**f**).

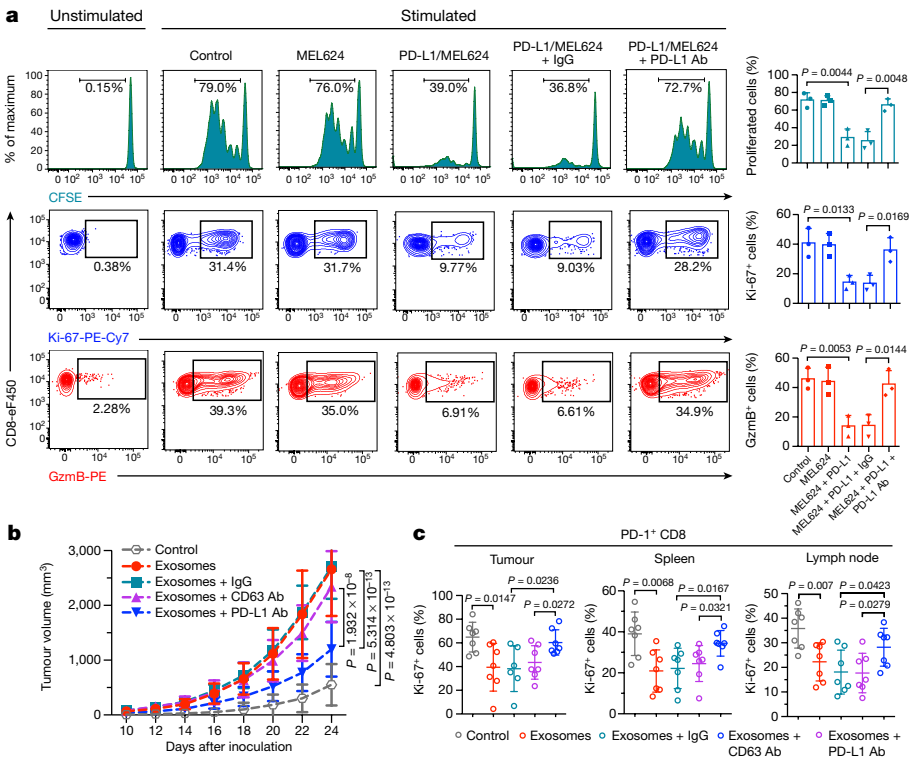

Fig. 3 | Exosomal PD-L1 inhibits CD8 T cells and facilitates the progression of melanoma in vitro and in vivo. a, Representative histogram of CFSE-labelled human peripheral CD8 T cells (top left) and representative contour plots of human peripheral CD8 T cells examined for the expression of Ki-67 (middle left) and granzyme B (GzmB) (bottom left) after indicated treatments. The proportions of cells with diluted CFSE dye, or positive Ki-67 or GzmB expression are shown on the right ($n = 3$ independent biological experiments). **b**, Growth curve of PD-L1(KD) B16-F10 tumours with indicated treatments ($n = 7$ mice per group). **c**, The proportions of Ki-67$^+$PD-1$^+$ CD8 TILs or splenic or lymph node CD8 T cells after indicated treatments ($n = 6$ for tumour samples of the EXO-IgG group, and $n = 7$ for all the other groups). See Extended Data Fig. 8d for representative contour plots. Data are mean ± s.d. (**a**–**c**). *P* values are from a two-sided unpaired *t*-test (**a**, **c**) or two-way ANOVA (**b**).

the level of circulating exosomal PD-L1 best distinguished melanoma patients from healthy donors (Fig. 2d–g, Extended Data Fig. 3e, f).

The current model for PD-L1-mediated immunosuppression is based on the interaction between PD-L1 on the tumour cell surface and PD-1 on CD8 T cells. Here we tested whether exosomal PD-L1 inhibits CD8 T cells. First, we used confocal microscopy to show a physical interaction between tumour exosomes and CD8 T cells purified from human peripheral blood (Extended Data Fig. 4a, b). Flow cytometry analyses further indicated that the level of interaction was higher for activated CD8 T cells than for non-activated counterparts (Extended Data Fig. 4c). Moreover, exosomes derived from melanoma cells treated with IFN-γ exhibited a higher level of binding to CD8 T cells (Extended Data Fig. 4d). Next, we tested the effect of exosomal PD-L1 on CD8 T cells, taking advantage of MEL624 cells, which do not express endogenous PD-L1 (Extended Data Fig. 5a–d) and other immunosuppressive proteins such as FasL and TRAIL[1]. Exosomes derived from MEL624 cells expressing exogenous PD-L1 inhibited the proliferation, cytokine production and cytotoxicity of CD8 T cells, as demonstrated by the decreased proportion of cells containing diluted carboxyfluorescein succinimidyl ester (CFSE, a cell division-tracking dye), reduced expression of Ki-67 and granzyme B (GzmB), and the inhibited production of IFN-γ, IL-2, and TNF (Fig. 3a, Extended Data Fig. 5e, f). Pre-treatment of the exosomes with anti-PD-L1 antibodies nearly abolished these effects. Similar effects were observed using exosomes secreted from WM9 cells, which express endogenous PD-L1 (Extended Data Fig. 5e–h). Exosomes derived from mouse melanoma B16-F10 cells also inhibited the proliferation and cytotoxicity of mouse splenic CD8 T cells (Extended Data Fig. 6a–d). Pre-treating OT-I T cells (which specifically recognize OVA peptide) (Extended Data Fig. 6e) with B16-F10 cell-derived exosomes inhibited their ability to kill their target cells (Extended Data Fig. 6f). Extracellular vesicles from human lung and breast cancer cells also contain immunosuppressive PD-L1, mostly of which is in exosomes, and PD-L1 expression is also upregulated by IFN-γ in some of these cell lines (Extended Data Fig. 7a–e).

To examine the effects of exosomal PD-L1 in vivo, we established a syngeneic mouse melanoma model in C57BL/6 mice using B16-F10 cells in which PD-L1 expression had been knocked down (PD-L1(KD) B16-F10) (Extended Data Fig. 8a). Injection of exosomes derived from parental B16-F10 cells promoted the growth of tumours derived from PD-L1(KD) B16-F10 cells, whereas pre-treatment of the exosomes with anti-PD-L1 antibodies, but not with IgG isotype or CD63-blocking antibodies, inhibited the effect (Fig. 3b, Extended Data Fig. 8b, c). The number of tumour-infiltrating CD8 T lymphocytes (TILs) decreased significantly after the injection of exosomes (Fig. 3c, Extended Data Fig. 8d, e). B16-F10 exosomes also decreased the proportion of proliferating PD-1$^+$ CD8 T cells in both spleen and lymph nodes (Fig. 3c, Extended Data Fig. 8d), suggesting that exosomal PD-L1 suppresses anti-tumour immunity systemically.

We then examined the level of PD-L1 on circulating extracellular vesicles in melanoma patients during anti-PD-1 therapy. The pre-treatment level of circulating exosomal PD-L1 was significantly higher in patients who failed to respond to the anti-PD-1 treatment with pembrolizumab (Fig. 4a). The difference was, however, not significant for total circulating PD-L1, and undetectable for PD-L1 on circulating microvesicles, or extracellular vesicle-excluded PD-L1 (Fig. 4b–d). A higher level of circulating exosomal PD-L1 before the treatment was associated with poorer clinical outcomes (Fig. 4e). IFN-γ upregulates exosomal PD-L1 and the pre-treatment levels of IFN-γ were significantly higher in patients who did not respond to pembrolizumab[21]. The level of circulating exosomal PD-L1 positively correlated with the level of circulating IFN-γ and overall tumour burden (Fig. 4f, g), which were shown to be indicative of poor prognosis[21].

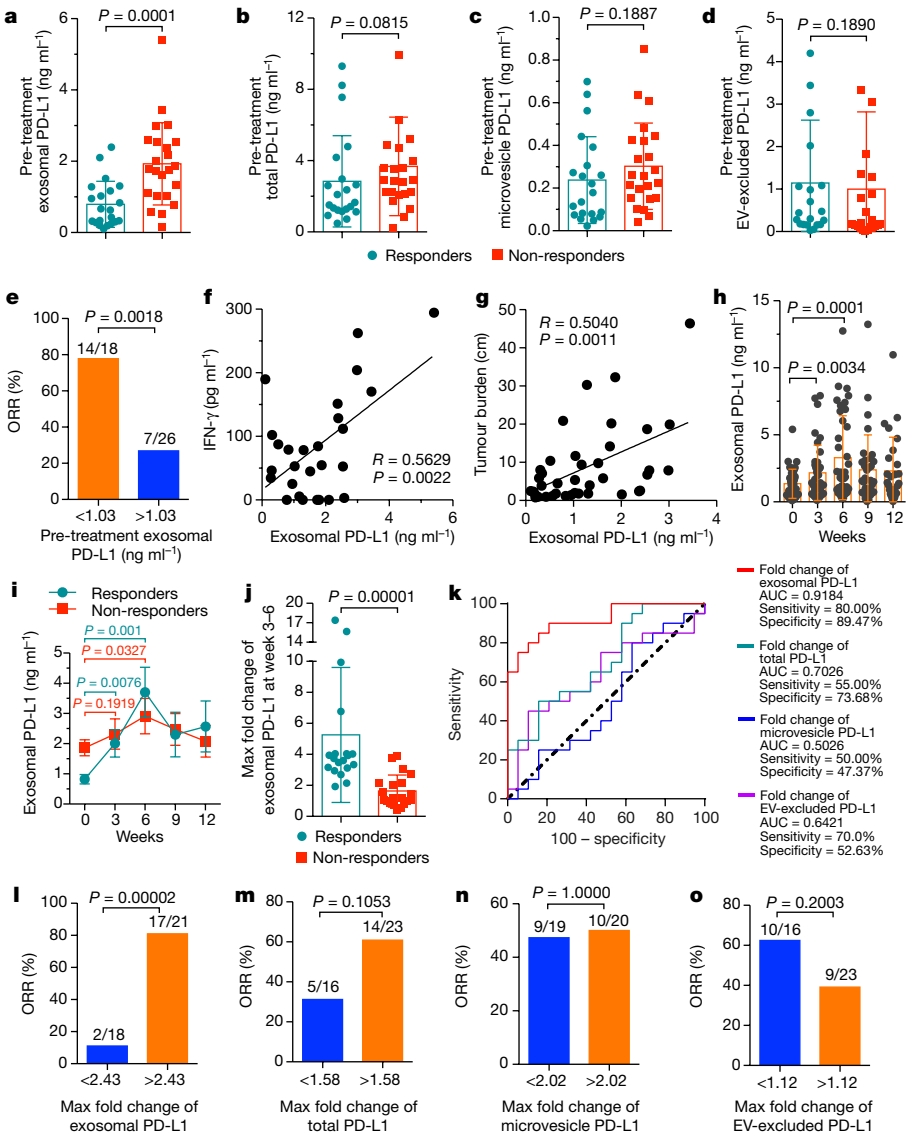

Fig. 4 | The level of circulating exosomal PD-L1 stratifies clinical responders to pembrolizumab and non-responders. **a**–**d**, Comparison of the pre-treatment levels of circulating exosomal PD-L1 (**a**), total PD-L1 (**b**), microvesicle PD-L1 (**c**), or extracellular vesicle-excluded PD-L1 (**d**) between melanoma patients with or without clinical response to pembrolizumab. R, responders; $n = 21$; NR, non-responders; $n = 23$. **e**, Objective response rate (ORR) for patients with high and low pre-treatment levels of circulating exosomal PD-L1. **f**, **g**, Pearson correlation of the IFN-γ level (**f**, $n = 27$) or overall tumour burden (**g**, $n = 39$) to the exosomal PD-L1 level in the plasma of patients with melanoma. **h**, Circulating exosomal PD-L1 at serial time points pre-treatment and on-treatment ($n = 39$). **i**, Circulating exosomal PD-L1 in clinical responders ($n = 19$) and non-responders ($n = 20$) at serial time points pre- and on-treatment. **j**, Comparison of the maximum fold change of circulating exosomal PD-L1 at week 3–6 between clinical responders and non-responders. **k**, ROC curve analysis for the maximum fold change of circulating exosomal PD-L1 at week 3–6 in clinical responders compared to non-responders. AUC, area under curve. **l**–**o**, ORR for patients with high and low fold changes of circulating exosomal PD-L1 (**l**), total PD-L1 (**m**), microvesicle PD-L1 (**n**), or extracellular vesicle-excluded PD-L1 (**o**), at weeks 3–6 of treatment. Data are mean ± s.d. $^*P < 0.05$, two-sided unpaired *t*-test (**a**–**d**, **j**), two-sided paired *t*-test (**h**, **i**), or two-sided Fisher's exact test (**e**, **l**–**o**).

Next, we examined the level of circulating exosomal PD-L1 in patients undergoing pembrolizumab therapy. In clinical responders, there were increased levels of PD-L1 on circulating exosomes, mostly within 6 weeks of therapy (Fig. 4h, i). The level of PD-L1 on microvesicles also increased in the same cohort of patients, but to a lesser extent in comparison to exosomes (Extended Data Fig. 9a). Proliferation and reinvigoration of CD8 T cells peaked at week 3 of treatment and preceded the peaking of exosomal PD-L1 at week 6 (Extended Data Fig. 9b). Moreover, in pembrolizumab-responsive patients, both the absolute value and maximal fold change of Ki-67 in PD-1$^+$ CD8 T cells after 3–6 weeks of treatment positively correlated with those of circulating exosomal PD-L1 (Extended Data Fig. 9c, d). The responders displayed a larger increase in the level of circulating exosomal PD-L1 as early as 3–6 weeks following the initial treatment (Fig. 4j). ROC analysis determined that a fold change of 2.43 in exosomal PD-L1 at week 3–6 stratified patients by clinical response to pembrolizumab (Fig. 4k); a fold change in circulating exosomal PD-L1 greater than 2.43 at week 3–6 was associated with a better response to anti-PD-1 therapy by objective response rate (ORR), progression-free and overall survival (Fig. 4l, Extended Data Fig. 9e). The fold increase of total circulating PD-L1, microvesicle PD-L1, and extracellular vesicle-excluded PD-L1 was inferior to that of exosomal PD-L1 for distinguishing responders from non-responders (Fig. 4k, m–o, Extended Data Fig. 9f–h).

Our studies suggest that melanoma cells release PD-L1-positive extracellular vesicles into the tumour microenvironment and circulation to counter the anti-tumour immunity systemically. Since exosomal PD-L1-mediated T cell inhibition can be blocked by antibodies against either PD-L1 or PD-1, our results raise the possibility that disrupting the interaction between exosomal PD-L1 and PD-1 on T cells is a previously unrecognized mechanism in PD-L1/PD-1 blockade-based therapies. The level of PD-L1 on extracellular vesicles is upregulated by IFN-γ, and PD-L1 on extracellular vesicles primarily targets PD-1$^+$ CD8 T cells, which represent the antigen-experienced T cells that secrete IFN-γ. Exosomal PD-L1 may therefore reflect the dynamic interplay between tumour and immune cells. Besides PD-L1, other extracellular vesicle proteins such as FasL may also contribute to immunosuppressive effects[19,22–24]. However, PD-L1 enables exosomes to target predominantly PD-1$^+$ CD8 T cells, allowing tumour cells to counteract the immune pressure at the effector stage. In addition to the interaction between exosomal-PD-L1 and PD-1, the involvement of other molecules including B7 and CD28[25,26] in this process also warrant investigation.

Our study suggests that circulating exosomal PD-L1 prior to and during pembrolizumab treatment may reflect distinct states of anti-tumour immunity. The pre-treatment PD-L1 level may correlate with a role of exosomal PD-L1 in immune dysfunction. High levels of exosomal PD-L1 may reflect the 'exhaustion' of T cells to a stage at which they can no longer be reinvigorated by anti-PD-1 treatment. In on-treatment patients, however, an increase in the level of exosomal PD-L1, following and correlating positively with T cell reinvigoration,

would reflect the presence of a successful anti-tumour immunity elicited by the anti-PD-1 therapy. Although the increase in exosomal PD-L1 in response to IFN-γ could enable tumour cells to adaptively inactivate CD8 T cells, this is futile because the interaction between PD-L1 and PD-1 is blocked by pembrolizumab. We observed no marked increase in exosomal PD-L1 in non-responders. This could be a result of failure to elicit an adequate T cell response, or a resistance mechanism to IFN-γ from tumours. Tumour cells in non-responders may have adaptively downregulated their response to IFN-γ to avoid the detrimental increase in antigen presentation and to escape the anti-proliferative effects induced by IFN-γ[5,27].

Our study offers a rationale for developing circulating exosomal PD-L1 as a predictor for the clinical outcomes of anti-PD-1 therapy, and sheds light on possible causes for the failure of anti-PD-1 therapies experienced by many patients (Extended Data Fig. 10). Tumour PD-L1 has been used as a predictive biomarker for clinical responses to anti-PD-1 therapy[28–30]. Considering the heterogeneity and dynamic changes of PD-L1 expression in tumours, and the invasive nature of tumour biopsy, developing exosomal PD-L1 as a blood-based biomarker could be an attractive option.

Online content

Any Methods, including any statements of data availability and Nature Research reporting summaries, along with any additional references and Source Data files, are available in the online version of the paper at https://doi.org/10.1038/s41586-018-0392-8.

Received: 16 October 2017; Accepted: 13 June 2018;
Published online 8 August 2018.

1. Dong, H. et al. Tumor-associated B7–H1 promotes T-cell apoptosis: a potential mechanism of immune evasion. *Nat. Med.* **8**, 793–800 (2002).
2. Chen, L. & Han, X. Anti-PD-1/PD-L1 therapy of human cancer: past, present, and future. *J. Clin. Invest.* **125**, 3384–3391 (2015).
3. Topalian, S. L., Taube, J. M., Anders, R. A. & Pardoll, D. M. Mechanism-driven biomarkers to guide immune checkpoint blockade in cancer therapy. *Nat. Rev. Cancer* **16**, 275–287 (2016).
4. Ribas, A. et al. Association of pembrolizumab with tumor response and survival among patients with advanced melanoma. *J. Am. Med. Assoc.* **315**, 1600–1609 (2016).
5. Zaretsky, J. M. et al. Mutations associated with acquired resistance to PD-1 blockade in melanoma. *N. Engl. J. Med.* **375**, 819–829 (2016).
6. Becker, A. et al. Extracellular vesicles in cancer: cell-to-cell mediators of metastasis. *Cancer Cell* **30**, 836–848 (2016).
7. Kalluri, R. The biology and function of exosomes in cancer. *J. Clin. Invest.* **126**, 1208–1215 (2016).
8. Robbins, P. D. & Morelli, A. E. Regulation of immune responses by extracellular vesicles. *Nat. Rev. Immunol.* **14**, 195–208 (2014).
9. Thery, C., Amigorena, S., Raposo, G. & Clayton, A. Isolation and characterization of exosomes from cell culture supernatants and biological fluids. *Curr. Protoc. Cell Biol.* **30**, 3.22.1–3.22.29 (2006).
10. Colombo, M., Raposo, G. & Thery, C. Biogenesis, secretion, and intercellular interactions of exosomes and other extracellular vesicles. *Annu. Rev. Cell Dev. Biol.* **30**, 255–289 (2014).
11. Peinado, H. et al. Melanoma exosomes educate bone marrow progenitor cells toward a pro-metastatic phenotype through MET. *Nat. Med.* **18**, 883–891 (2012).
12. Melo, S. A. et al. Glypican-1 identifies cancer exosomes and detects early pancreatic cancer. *Nature* **523**, 177–182 (2015).
13. Tibes, R. et al. Reverse phase protein array: validation of a novel proteomic technology and utility for analysis of primary leukemia specimens and hematopoietic stem cells. *Mol. Cancer Ther.* **5**, 2512–2521 (2006).
14. Garcia-Diaz, A. et al. Interferon receptor signaling pathways regulating PD-L1 and PD-L2 expression. *Cell Reports* **19**, 1189–1201 (2017).
15. Schmidt, O. & Teis, D. The ESCRT machinery. *Curr. Biol.* **22**, R116–R120 (2012).
16. Ostrowski, M. et al. Rab27a and Rab27b control different steps of the exosome secretion pathway. *Nat. Cell Biol.* **12**, 19–30 (2010).
17. Zhou, J. et al. Soluble PD-L1 as a biomarker in malignant melanoma treated with checkpoint blockade. *Cancer Immunol. Res.* **5**, 480–492 (2017).
18. Theodoraki, M. N., Yerneni, S. S., Hoffmann, T. K., Gooding, W. E. & Whiteside, T. L. Clinical significance of PD-L1$^+$ exosomes in plasma of head and neck cancer patients. *Clin. Cancer Res.* **24**, 896–905 (2018).
19. Ludwig, S. et al. Suppression of lymphocyte functions by plasma exosomes correlates with disease activity in patients with head and neck cancer. *Clin. Cancer Res.* **23**, 4843–4854 (2017).
20. Ricklefs, F. L. et al. Immune evasion mediated by PD-L1 on glioblastoma-derived extracellular vesicles. *Sci. Adv.* **4**, eaar2766 (2018).
21. Huang, A. C. et al. T-cell invigoration to tumour burden ratio associated with anti-PD-1 response. *Nature* **545**, 60–65 (2017).
22. Kim, J. W. et al. Fas ligand-positive membranous vesicles isolated from sera of patients with oral cancer induce apoptosis of activated T lymphocytes. *Clin. Cancer Res.* **11**, 1010–1020 (2005).
23. Strauss, L., Bergmann, C. & Whiteside, T. L. Human circulating CD4$^+$CD25^{high}Foxp3$^+$ regulatory T cells kill autologous CD8$^+$ but not CD4$^+$ responder cells by Fas-mediated apoptosis. *J. Immunol.* **182**, 1469–1480 (2009).
24. Wieckowski, E. U. et al. Tumor-derived microvesicles promote regulatory T cell expansion and induce apoptosis in tumor-reactive activated CD8$^+$ T lymphocytes. *J. Immunol.* **183**, 3720–3730 (2009).
25. Kamphorst, A. O. et al. Rescue of exhausted CD8 T cells by PD-1-targeted therapies is CD28-dependent. *Science* **355**, 1423–1427 (2017).
26. Hui, E. et al. T cell costimulatory receptor CD28 is a primary target for PD-1-mediated inhibition. *Science* **355**, 1428–1433 (2017).
27. Shin, D. S. et al. Primary Resistance to PD-1 Blockade Mediated by JAK1/2 Mutations. *Cancer Discov.* **7**, 188–201 (2017).
28. Reck, M. et al. Pembrolizumab versus chemotherapy for PD-L1-positive non-small-cell lung cancer. *N. Engl. J. Med.* **375**, 1823–1833 (2016).
29. Patel, S. P. & Kurzrock, R. PD-L1 expression as a predictive biomarker in cancer immunotherapy. *Mol. Cancer Ther.* **14**, 847–856 (2015).
30. Tumeh, P. C. et al. PD-1 blockade induces responses by inhibiting adaptive immune resistance. *Nature* **515**, 568–571 (2014).

Acknowledgements We thank S. Fuchs and J. Ridley (University of Pennsylvania) for their helpful comments. This work is supported by NIH grants GM111128 and GM085146 to W.G., AI105343, AI108545, AI082630, AI117950, Parker Institute for Cancer Immunotherapy to E.J.W., 2T32CA009615-26 to A.C.H., American Heart Association to G.C., CA114046, CA025874, CA010815, CA193417, CA047159, P50 CA174523 (SPORE) and the Tara Miller Foundation to M.H., L.M.S., G.C.K., T.C.M., W.G., X.Xu., the University of Pennsylvania and the Wistar Institute, the Dr. Miriam and Sheldon G. Adelson Medical Research Foundation to M.H., the CAST foundation 2016QNRC001, 2015QNRC001 to Wuhan University, and the NSFC foundation 81570994 to Y.Z.

Reviewer information *Nature* thanks H. Peinado, T. Tueting and the other anonymous reviewer(s) for their contribution to the peer review of this work.

Author contributions G.C. and W.G. conceived the project and designed the experiments. G.C., W.Zha., M.W., Z.Y., J.Y., H.X., Q.M., W.Zho. and X.Xi. purified and characterized extracellular vesicles. G.C., W.Zha., J.Y., B.Wa., W.Zho., X.L., S.L. and L.D. performed the mice experiments. G.C., W.Zha., M.W., J.Y., B.Wa. and B.Wu performed the immunoprecipitation and western blot analysis. G.C., A.C.H., M.W., J.Y., H.S. and R.Y. performed the flow cytometry experiments. G.C., W.Zha. and J.Y. performed the nanoparticle tracking, ELISAs, qPCR, PD-1 binding and immunofluorescence staining experiments. G.C., Z.Y., H.X. and Q.M. performed the electron microscopy experiments. G.C., W.Zha., H.S. and J.Y. performed the T cell proliferation and tumour-killing experiments. G.C., H.S., L.G. and T.L. generated the bone marrow-derived dendritic cells and performed the antigen cross-presentation experiments. G.M. and Yi.L. performed the RPPA experiments. G.C.K. and X.Xu. performed pathological analyses. W.X., L.F.A., S.M., R.S., T.C.M. and L.M.S. provided human samples and associated clinical data. H.D. and M.H. provided melanoma cell lines. G.C., A.C.H., W.Zha., G.Z., M.W., W.X., Z.Y., Yo.L., R.R., G.M., J.K., Y.H.C., H.D., Y.Z., T.C.M., L.M.S., E.J.W., X.Xu. and W.G. analysed and interpreted the data. G.C. and W.G. wrote the paper. G.Z., A.C.H., Y.H.C., H.D., M.H., E.J.W. and X.Xu. edited the paper. All authors have read and approved the final manuscript.

Competing interests W.G., G.C. and X.Xu. are listed as inventors on a patent owned by the University of Pennsylvania related to this work. W.G. and X.Xu. serve on the Scientific Advisory Board and have equities in Exo Bio, a company that has licensed the patent from the University of Pennsylvania.

Additional information
Extended data is available for this paper at https://doi.org/10.1038/s41586-018-0392-8.
Supplementary information is available for this paper at https://doi.org/10.1038/s41586-018-0392-8.
Reprints and permissions information is available at http://www.nature.com/reprints.
Correspondence and requests for materials should be addressed to X.Xu. or W.G.
Publisher's note: Springer Nature remains neutral with regard to jurisdictional claims in published maps and institutional affiliations.

METHODS

Cell culture. The A375 human melanoma and B16-F10 mouse melanoma cells were purchased from ATCC. The control and PD-L1-overexpressing human melanoma MEL624 cells were provided by H. Dong (Mayo Clinic). Mouse melanoma B16 cells stably expressing chicken OVA (B16-OVA) were provided by H. C. J. Ertl (The Wistar Institute). The UACC-903 human melanoma cells were provided by M. Powell (Stanford University). The melanoma cell lines WM1552C, WM35, WM793, WM902B, WM9 and WM164 presented in this study were established in M. Herlyn's laboratory (The Wistar Institute). All cell lines were authenticated by DNA fingerprinting, and were tested routinely before use to avoid mycoplasma contamination. Human melanoma cell lines MEL624, PD-L1/MEL624, WM1552C, WM35, WM902B, WM793, UACC-903, WM9, A375 and WM164 were cultured in RPMI 1640 medium (Invitrogen) supplemented with 10% (v/v) fetal bovine serum (FBS) (Invitrogen). B16-F10 and B16-OVA cells were cultured in DMEM (Sigma) supplemented with 10% (v/v) FBS. For stimulation with IFN-γ, cells were incubated with 100 ng/ml of recombinant human or mouse IFN-γ (Peprotech) for 48 h.

Generation of stable Hrs, Rab27a or PD-L1 knockdown melanoma cells. Short hairpin RNAs (shRNAs) against human *Hrs* (also known as *HGS*) (NM_004712, GCACGTCTTTCCAGAATTCAA, GCATGAAGAGTAACCACAGC), human *RAB27A* (NM_004850, GCTGCCAATGGGACAAACATA, CAGGAGAGGTTT CGTAGCTA) (gift from A. Weaver, Vanderbilt University), mouse *PD-L1* (also known as *Cd274*) (NM_021893, GCGTTGAAGATACAAGCTCAA) or scrambled shRNA-control (Addgene) were packaged into lentiviral particles using 293T cells co-transfected with the viral packaging plasmids. Lentiviral supernatants were harvested 48–72 h after transfection. Cells were infected with filtered lentivirus and selected by 2 μg/ml puromycin.

Patients and specimen collection. Patients with stage III to IV melanoma (Supplementary Table 1) were enrolled for treatment with pembrolizumab (2 mg/kg by infusion every 3 weeks) under an Expanded Access Program at Penn (http://clinicaltrials.gov identifier NCT02083484) or with commercial Keytruda. Patients gave consent in writing for blood collection under the University of Pennsylvania Abramson Cancer Center's melanoma research program tissue collection protocol UPCC 08607 in accordance with the ethics committee and The Institutional Review Board of the University of Pennsylvania. Peripheral blood was obtained in sodium heparin tubes before each pembrolizumab infusion every 3 weeks for 12 weeks. Clinical response was determined as best response based on immune-related RECIST (irRECIST) using unidimensional measurements[31]. The assessment of clinical responses for patients was performed independently in a double-blind fashion. Blood samples from healthy donors were collected at The Wistar Institute after approval by the ethics committee and Institutional Review Board of The Wistar Institute. Written consent was obtained from each healthy donor before blood collection. All experiments involving blood samples from healthy donors were performed in accordance with relevant ethical regulations.

Flow cytometry of patients' PBMCs. Peripheral blood mononuclear cells (PBMCs) were isolated using Ficoll gradient and stored using standard protocols. Cryopreserved PBMC samples from pretreatment, cycles 1–4 (weeks 3–12) were thawed and analysed by flow cytometry as previously described[21]. In brief, live or dead cell discrimination was performed using Live/Dead Fixable Aqua Dead Cell Stain Kit (Life Technologies). Cell surface staining was performed for 30 min at 4 °C. Intracellular staining was performed for 60 min on ice after using a fixation/permeabilization kit (eBioscience).

Purification of extracellular vesicles. For exosome purification from cell culture supernatants, cells were cultured in media supplemented with 10% exosome-depleted FBS. Bovine exosomes were depleted by overnight centrifugation at 100,000*g*. Supernatants were collected from 48–72 h cell cultures and extracellular vesicles were purified by a standard differential centrifugation protocol[9–12]. In brief, culture supernatants were centrifuged at 2,000*g* for 20 min to remove cell debris and dead cells (Beckman Coulter, Allegra X-14R). Microvesicles were pelleted after centrifugation at 16,500*g* for 45 min (Beckman Coulter, J2-HS) and resuspended in PBS. Supernatants were then centrifuged at 100,000*g* for 2 h at 4 °C (Beckman Coulter, Optima XPN-100). The pelleted exosomes were suspended in PBS and collected by ultracentrifugation at 100,000*g* for 2 h.

For purification of circulating extracellular vesicles by differential centrifugation, venous citrated blood from melanoma patients or healthy donors was centrifuged at 1,550*g* for 30 min to obtain cell-free plasma (Beckman Coulter, Allegra X-14R). Then, 1 ml of the obtained plasma was centrifuged at 16,500*g* for 45 min (Eppendorf, 5418R). The pelleted microvesicles were suspended in PBS. The collected supernatants were then centrifuged at 100,000*g* for 2 h at 4 °C (Beckman Coulter, Optima™ MAX-XP) to pellet the exosomes. For purification of circulating exosomes using the exosome isolation kit, cell-free plasma was first centrifuged at 16,500*g* for 45 min (Eppendorf, 5418R) to pellet large membrane vesicles. Exosomes were then purified from the supernatants using the exosome isolation kit (Invitrogen, Cat# 4484450).

Characterization of purified exosomes. For verification of purified exosomes using electron microscopy, purified exosomes suspended in PBS were dropped on formvar carbon-coated nickel grids. After staining with 2% uranyl acetate, grids were air-dried and visualized using a JEM-1011 transmission electron microscope. For immunogold labelling, purified exosomes suspended in PBS were placed on formvar carbon-coated nickel grids, blocked, and incubated with mouse anti-human monoclonal antibody that recognizes the extracellular domain of PD-L1 (clone 5H1-A3)[1], followed by incubation with the anti-mouse secondary antibody conjugated with protein A-gold particles (5 nm). Each staining step was followed by five PBS washes and ten ddH_2O washes before contrast staining with 2% uranyl acetate.

The size and concentration of exosomes purified from cell culture supernatants or patients' plasma were determined using a NanoSight NS300 (Malvern Instruments), which is equipped with fast video capture and particle-tracking software.

For iodixanol density gradient centrifugation, exosomes harvested by differential centrifugation were loaded on top of a discontinuous iodixanol gradient (5%, 10%, 20% and 40%, made by diluting 60% OptiPrep aqueous iodixanol with 0.2 5M sucrose in 10 mM Tris) and centrifuged at 100,000*g* for 18 h at 4 °C (Beckman Coulter, Optima MAX-XP). Twelve fractions of equal volume were collected from the top of the gradients, with the exosomes distributed at the density range between 1.13 and 1.19 g/ml, as previously demonstrated[8,9,11,12]. The exosomes were further pelleted by ultracentrifugation at 100,000*g* for 2 h at 4 °C.

Immunoprecipitation. To analyse the role of ESCRT machinery in exosomal secretion of PD-L1 in melanoma cells, PD-L1/MEL624 cells were transfected with Flag-Hrs plasmid or vector and then lysed. The cleared lysate was incubated with Anti-FLAG Affinity Gel (Sigma-Aldrich) overnight at 4 °C. The immunoprecipitated proteins were resolved by SDS-polyacrylamide gel electrophoresis and transferred to nitrocellulose membranes. PD-L1 and Flag (Hrs) were determined by western blot using specific antibodies.

ELISA. For detection of PD-L1 on extracellular vesicles, cell supernatants or patients' plasma, ELISA plates (96-well) (Biolegend) were coated with 0.25 μg per well (100 μl) of monoclonal antibody against PD-L1 (clone 5H1-A3) overnight at 4 °C. Free binding sites were blocked with 200 μl of blocking buffer (Pierce) for 1 h at room temperature. Then, 100 μl of plasma samples with or without extracellular vesicle removal, or extracellular vesicle samples purified from plasma or cell culture supernatants, were added to each well. The exosome or microvesicle samples purified from cell culture supernatants were prepared by serial dilution according to the total protein level to analyse the enrichment of PD-L1 on exosomes and microvesicles. The concentration of PD-L1 on the surface of exosomes isolated from indicated cells was calculated based on the linear range of the ELISA assay data. The exosome or microvesicle samples derived from the plasma samples of healthy donors or melanoma patients were prepared using the same volume of PBS as the plasma as they were originally derived from. The plasma samples with (extracellular vesicle-excluded) or without (total) extracellular vesicle removal were diluted with PBS in a 1:0.75 volume ratio. After overnight incubation at 4 °C, biotinylated monoclonal PD-L1 antibody (clone MIH1, eBioscience) was added to each well and incubated for 1 h at room temperature. A total of 100 μl per well of horseradish peroxidase-conjugated streptavidin (BD Biosciences) diluted in PBS containing 0.1% BSA was then added and incubated for 1 h at room temperature. Plates were developed with tetramethylbenzidine (Pierce) and stopped with 0.5N H_2SO_4. The plates were read at 450 nm with a BioTek plate reader. Recombinant human PD-L1 protein (R&D Systems, Cat# 156-B7) was used to make a standard curve. Recombinant P-selectin protein (R&D Systems, Cat# 137-PS) was used as negative control to verify the detection specificity. The result of standard curve demonstrated that the established ELISA exhibited a reliable linear detection range from 0.2 to 12 ng/ml.

For detection of IFN-γ, TNF and IL-2, the supernatant of human CD8 T cells was harvested and measured according to the kit manufacturer's instructions (Biolegend).

PD-1–PD-L1 binding assay. To test the binding of exosomal PD-L1 to PD-1, 100 μl of exosome samples of different concentrations were captured onto PD-L1 antibody (clone 5H1-A3)-coated 96-well ELISA plates by overnight incubation at 4 °C. Then 100 μl of 4 μg/ml biotin-labelled human PD-1 protein (BPS Bioscience, Cat# 71109) was added and incubated for 2 h at room temperature. A total of 100 μl per well of horseradish peroxidase-conjugated streptavidin (BD Biosciences) diluted in PBS containing 0.1% BSA was then added and incubated for 1 h at room temperature. Plates were developed with tetramethylbenzidine (Pierce) and stopped using 0.5N H_2SO_4. The plates were read at 450 nm with a BioTek plate reader. Recombinant human PD-L1 protein directly coated onto the plates was used as the positive control.

Treatment of CD8 T cells with the exosomes. To block PD-L1 on the exosome surface, purified exosomes (200 μg) were incubated with PD-L1 blocking antibodies (10 μg/ml) or IgG isotype antibodies (10 μg/ml) in 100 μl PBS, and then washed with 30 ml PBS and pelleted by ultracentrifugation to remove the non-bound free antibodies. Human CD8 T cells purified from peripheral blood using

immunodepletion on a Ficoll-Hypaque gradient (RosetteSep, StemSep Technologies) or mouse CD8 T cells purified from splenocytes using Dynabeads Untouched Mouse CD8 Cells Kit (Invitrogen) were stimulated with anti-CD3 (2 μg/ml) and anti-CD28 (2 μg/ml) antibodies for 24 h and then incubated with human melanoma cell-derived exosomes or mouse B16-F10 cell-derived exosomes with or without PD-L1 blocking for 48 h in the presence of anti-CD3/CD28 antibodies. For human CD8 T cells (2×10^5 cells/well in a 96-well plate), 25 μg/ml of human WM9 cell-derived exosomes (carrying surface PD-L1 at a level of 0.05 ng per μg of exosomes as determined by ELISA, Fig. 1i) were used as the circulating exosomal PD-L1 level in melanoma patients is around 1.25 ng/ml (Fig. 2h). For mice CD8 T cells (2×10^5 cells/well in a 96-well plate), 100 μg/ml of mouse B16-F10 cell-derived exosomes (carrying surface PD-L1 at a level of 0.016 ng per μg of exosomes as determined by ELISA) were used as the circulating exosomal PD-L1 level in mice bearing B16-F10 tumours is around 1.63 ng/ml. The treated cells were then collected, stained, and analysed by flow cytometry. Information about the primary antibodies is included in Supplementary Table 2. To assay for the proliferation of CD8 T cells, CFSE, a dye for the tracking of cell division (Molecular Probes) was used. A total of 1×10^6 CD8 T cells were stained with CFSE at 5 μM. The cells were then incubated at 37 °C for 20 min and the reaction was stopped by adding 5 volumes of cold medium with 10% FBS, and treated as above. Unstimulated CFSE-labelled cells served as a non-dividing control.

The exosome–T cell binding assay. To verify the physical interactions between melanoma cell-derived exosomes and CD8 T cells, purified exosomes were stained with CFSE in 100 μl PBS, and then washed with 10 ml PBS and pelleted by ultracentrifugation. Unstimulated or stimulated human CD8 T cells (2×10^5 cells/well in 96-well plates) were treated with CFSE-labelled exosomes (25 μg/ml) for 2 h, and then fixed for flow cytometry or confocal microscopy after immunostaining for CD8 T cells.

Generation of dendritic cells from bone marrow. Dendritic cells (DCs) were generated from bone marrow of C57BL/6 mice and cultured in RPMI 1640 with 10% (v/v) FBS, 20 mM L-glutamine, 50 μM β-mercapoethanol, 20 ng/ml IL-4 and 20 ng/ml GM-CSF. After 3 days, half of the culture medium was replaced by fresh medium containing 40 ng/ml IL-4 and 40 ng/ml GM-CSF. To prime antigen-specific OT-I CD8 T cells, DCs were subsequently loaded with 2 μg/ml SIINFEKL ($OVA_{257–264}$) peptide overnight.

CD8 T cell-mediated tumour cell killing assay. To determine the effects of melanoma cell-derived exosomes on the ability of CD8 T cells to kill tumour cells, CD8 T cells were purified from the splenocytes of OT-I mice expressing a transgene encoding a T cell receptor that specifically recognized SIINFEKL peptide bound to MHC-I H-$2k^{b}$[32]. OT-I CD8 T cells (4×10^5 cells/well in a 48-well plate) were then activated by incubation with SIINFEK-loaded (2 μg/ml) bone marrow-derived DCs (2×10^5 cells/well). The activated OT-I CD8 T cells (4×10^5 cells/well in 48-well plate) were treated with PBS (as a control) or B16-F10-derived exosomes (100 μg/ml for 48 h) with or without IgG isotype or PD-L1 antibody blocking (10 μg/ml), and then co-cultured with CFSE-labelled melanoma PD-L1 (KD) B16/OVA cells (4×10^5) in 6-well plates for 48 h at an effector to target (E:T) ratio of 1:1. Cells were then harvested, intracellularly stained with BV650-conjugated antibody against cleaved-caspase-3 (BD Biosciences) and analysed by flow cytometry. Information about the primary antibodies is included in Supplementary Table 2.

Immunofluorescence staining. Immunofluorescence staining was performed on fixed cells or formalin-fixed, paraffin-embedded (FFPE) sections. For fixed cells, permeabilization with 0.1% Triton X-100 was performed before blocking with bovine serum albumin (BSA) buffer for 1 h. For FFPE sections, antigen retrieval by steaming in citrate buffer (pH = 6.0) was performed before blocking. The fixed cells or FFPE sections were incubated with primary antibodies overnight at 4 °C, followed by incubation with fluorophore-conjugated secondary antibodies for 1 h. Nuclei were stained with DAPI. Samples were observed using a Nikon confocal microscope at 100× magnification.

Western blot analysis. Whole cell lysates or exosomal proteins were separated using 12% SDS–PAGE and transferred onto nitrocellulose membranes. The blots were blocked with 5% non-fat dry milk at room temperature for 1 h, and incubated overnight at 4 °C with the corresponding primary antibodies at dilutions recommended by the suppliers, followed by incubation with HRP-conjugated secondary antibodies (Cell Signaling Technology) at room temperature for 1 h. The blots on the membranes were developed with ECL detection reagents (Pierce). CD63, Hrs, Alix, and TSG101 were used as exosome markers. TYRP-1 and TYRP-2 were used as melanoma-specific markers. GAPDH was used as a loading control. Information about the primary antibodies was included in Supplementary Table 2.

Quantitative PCR (qPCR). Total RNA was isolated from CD8 T cells using TRIzol Reagent (Invitrogen), and reverse transcribed into first-strand complementary DNA (cDNA) with random primer with RevertAid First Strand cDNA Synthesis Kit (ThermoFisher Scientific). The samples were then analysed in an Applied Biosystems QuantStudio 3 Real-Time PCR system. *GAPDH* was used as an internal control. Information about the primers is included in Supplementary Table 3.

In vivo mice study. All animal experiments were performed according to protocols approved by the Institutional Animal Care and Use Committee (IACUC) of the University of Pennsylvania. For establishing human melanoma xenograft model in nude mice, WM9 cells (5×10^6 cells in 100 μl medium) were injected into flanks of 8-week-old female athymic nude mice. Tumours were measured using a digital caliper and the tumour volume was calculated by the formula: $(\text{width})^2 \times \text{length}/2$. Mice were euthanized 30 days after cell inoculation or if the longest dimension of the tumours reached 2.0 cm before 30 days. Immediately following euthanasia, blood samples were harvested by cardiac puncture, and exosomes were purified and detected by ELISA using the aforementioned method. Exosomes purified from sex-, age- and weight-matched healthy nude mice without xenograft were used as the control.

For establishing syngeneic mouse melanoma model in C57BL/6 mice, B16-F10 cells or B16-F10 PD-L1 (KD) cells (5×10^5 cells in 100 μl medium) were subcutaneously injected into immunocompetent C57BL/6 mice. Based on the difference in the level of circulating exosomal PD-L1 between mice bearing parental B16-F10 and PD-L1 (KD) B16-F10 tumours (1.63 ng/ml vs 0.70 ng/ml), a total of 100 μg of parental B16-F10 cell-derived exosomes (carrying surface PD-L1 at a level of 0.016 ng per μg of exosomes) with or without IgG isotype, CD63 or PD-L1 blocking (10 μg/ml) were injected into mice after inoculation of PD-L1 (KD) B16-F10 cells to examine the functional significance of PD-L1. The dose of 100 μg exosomes used for our in vivo study was equivalent to approximately 30% of the physiological level of circulating exosomes in mice, and was also comparable to those from a palpable tumour in mice according to our data. Tail vein injections of exosomes (100 μg in 100 μl PBS) were performed every 3 days. Mice were weighed every 3 days. Tumours were measured using a digital caliper and the tumour volume was calculated by the formula: $(\text{width})^2 \times \text{length}/2$. The mice were euthanized before the longest dimension of the tumours reached 2.0 cm. Mice were allocated randomly to each treatment group. Downstream analyses of mouse samples (immunofluorescence staining, flow cytometry and ELISA) were performed in a blinded fashion. For flow cytometry, the spleen and tumour samples were harvested, and single cell suspensions were prepared and red blood cells were lysed using ACK Lysis Buffer. Information about the primary antibodies is included in Supplementary Table 2.

Reverse phase protein array (RPPA). RPPA was performed at the MD Anderson Cancer Center core facility using 50 μg protein per sample. All of the antibodies were validated by western blot[13]. Methods for data analysis are described below.

Statistical analyses. RPPA data analysis was performed according to the protocol from the MD Anderson Cancer Center. Specifically, relative protein levels for each sample were determined by interpolation of each dilution curve from the 'standard curve' (supercurve) of the slide (antibody). Supercurve is constructed by a script in R written by the RPPA core facility. The package binaries of SuperCurve and SuperCurveGUI are available in R-Forge (https://r-forge.r-project.org/R/?group_id=1899). These values are defined as supercurve $\log_2$ value. All the data points were normalized for protein loading and transformed to linear value, designated as 'normalized linear'. Normalized linear value was transformed to the $\log_2$ value, and then median-centred for further analysis. Median-centred values were obtained by subtracting the median of all samples in a given protein. All of the above-mentioned procedures were performed by the RPPA core facility. The normalized data provided by the RPPA core facility were analysed by Cluster 3.0 (http://bonsai.ims.u-tokyo.ac.jp/~mdehoon/software/cluster/) and visualized using the Java TreeView 1.0.5 (http://jtreeview.sourceforge.net/).

All other statistical analyses were performed using GraphPad Prism v.6.0. Normality of distribution was determined by D'Agostino–Pearson omnibus normality test and variance between groups was assessed by the *F*-test. For normally distributed data, significance of mean differences was determined using two-tailed paired or unpaired Student's *t*-tests; for groups that differed in variance, unpaired *t*-test with Welch's correction was performed. For data that were not normally distributed, non-parametric Mann–Whitney *U*-tests or Wilcoxon matched-pairs tests were used for unpaired and paired analysis, respectively. Correlations were determined by Pearson's *r* coefficient. Two-way ANOVA was used to compare mouse tumour volume data among different groups. log-rank and Wilcoxon tests were used to analyse the mouse survival data. Error bars shown in graphical data represent mean ± s.d. A two-tailed value of $P < 0.05$ was considered statistically significant.

Reporting summary. Further information on experimental design is available in the Nature Research Reporting Summary linked to this paper.

Data availability. All data and materials are available from the authors upon reasonable request.

31. Nishino, M. et al. Developing a common language for tumor response to immunotherapy: immune-related response criteria using unidimensional measurements. *Clin. Cancer Res.* **19**, 3936–3943 (2013).
32. Hogquist, K. A. et al. T cell receptor antagonist peptides induce positive selection. *Cell* **76**, 17–27 (1994).

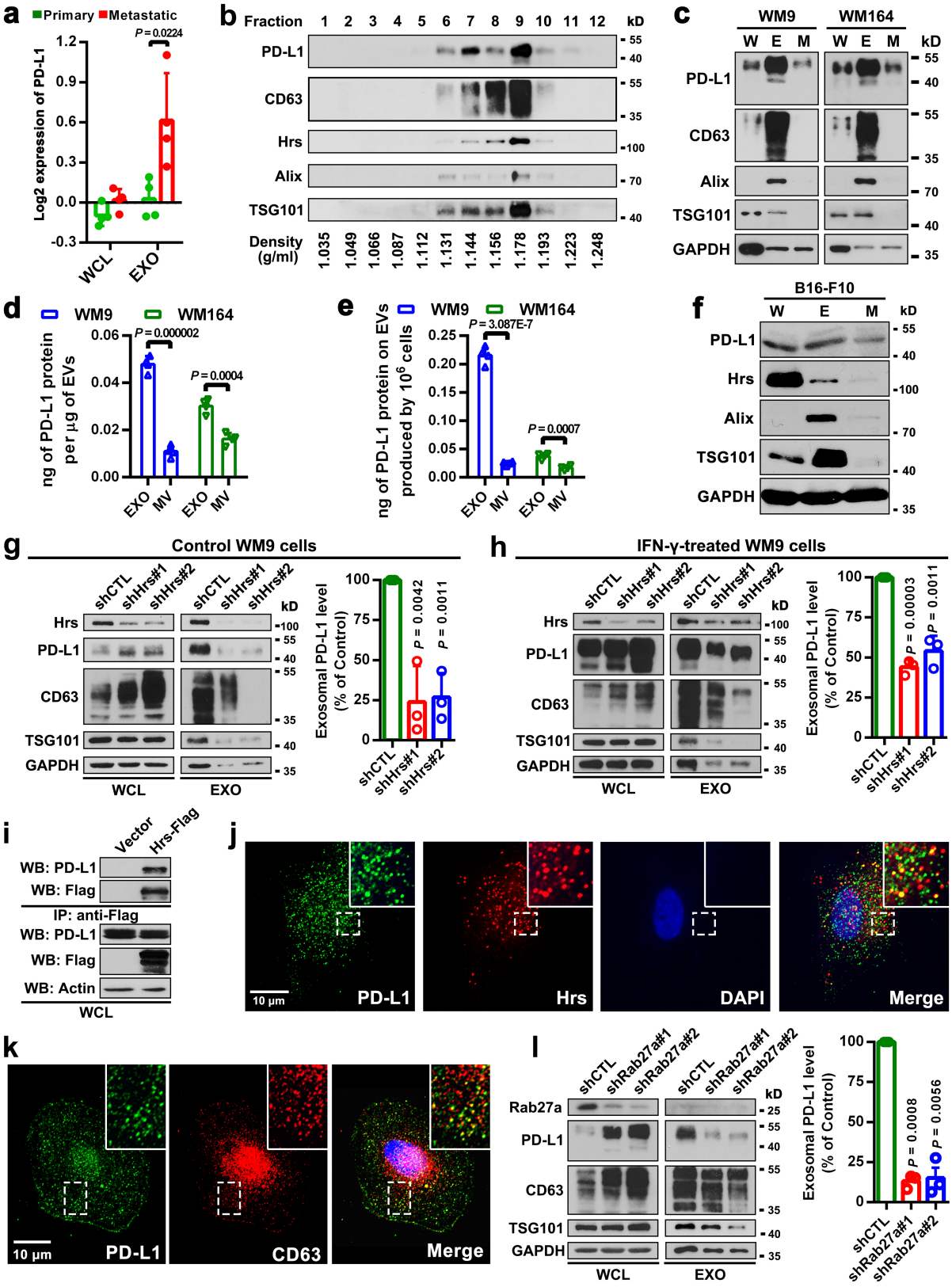

Extended Data Fig. 1 | See next page for caption.

Extended Data Fig. 1 | Melanoma cells release extracellular vesicles carrying PD-L1. a, The log_2-transformed RPPA data showing a higher level of exosomal PD-L1 secreted by metastatic melanoma cell lines compared with primary melanoma cell lines. Data represent mean ± s.d. of four primary (WM1552C, WM35, WM793, WM902B) or metastatic (UACC-903, 1205Lu, WM9, WM164) melanoma lines. **b**, Density gradient centrifugation confirming that PD-L1 secreted by WM9 cells co-fractionated with exosome markers CD63, Hrs, Alix and TSG101. **c**, Immunoblots for PD-L1 in the whole cell lysate (W), purified exosomes (E) or microvesicles (M) from different metastatic melanoma cell lines. The same amount of protein was loaded in each lane. **d**, Levels of PD-L1 on the exosomes or microvesicles derived from melanoma cells as assayed by ELISA. **e**, The levels of exosomal PD-L1 and microvesicle PD-L1 produced by an equal number of melanoma cells. **f**, Immunoblots for PD-L1 in the whole cell lysate, purified exosomes or microvesicles from mouse melanoma B16-F10 cells. The same amount of protein was loaded in each lane. **g**, **h**, Western blot analysis of PD-L1 in *Hrs* knockdown cells without (**g**) or with (**h**) IFN-γ treatment. Quantification of the western blotting data (**g**, right; **h**, right). **i**, Co-immunoprecipitation of PD-L1 and Hrs from MEL624 cells expressing exogenous PD-L1 and Hrs. **j**, Immunofluorescence staining of intracellular PD-L1 and exosome marker Hrs in WM9 cells treated with IFN-γ. **k**, Immunofluorescence staining of intracellular PD-L1 and CD63 in WM9 cells treated with IFN-γ. **l**, western blotting analysis showing intracellular accumulation of PD-L1, and decreased exosomal secretion of PD-L1 in WM9 cells with *RAB27A* knockdown (left). The levels of exosomal PD-L1 were compared (right). Two experiments were repeated independently with similar results (**b**, **c**, **f**, **i**–**k**). Data represent mean ± s.d. of four (**d**, **e**), or three (**g**, **h**, **l**) independent biological replicates. Statistical analysis is performed by two-sided unpaired *t*-test (**a**, **d**, **e**, **g**, **h**, **l**). For gel source data (**b**, **c**, **f**–**i**, **l**), see Supplementary Fig. 1.

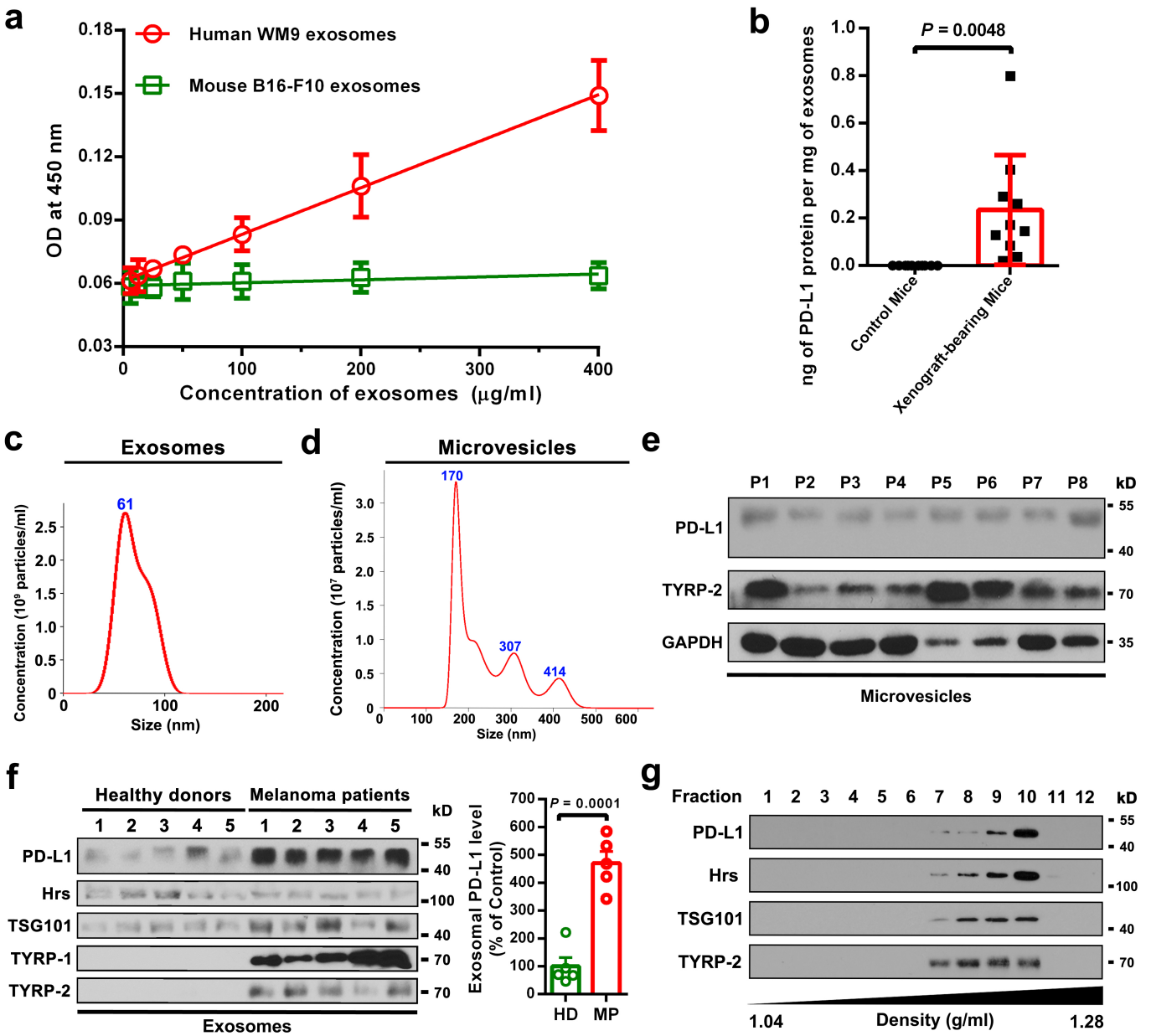

Extended Data Fig. 2 | Melanoma cells secrete exosomal PD-L1 into the circulation. a, The monoclonal antibodies against the extracellular domain of human PD-L1 specifically detect human exosomal PD-L1, but not mouse exosomal PD-L1 ($n = 3$ biologically independent experiments). **b**, Levels of human PD-L1 in exosomes from the plasma of control nude mice ($n = 10$) and human WM9 melanoma xenograft-bearing nude mice ($n = 10$) per mg of total circulating exosomal proteins. **c**, Characterization of circulating exosomes purified from the plasma of a patient with Stage IV melanoma using NanoSight nanoparticle tracking analysis. **d**, Characterization of circulating microvesicles purified from the plasma sample of a patient with Stage IV melanoma using NanoSight nanoparticle tracking analysis. **e**, Immunoblots for PD-L1 in the microvesicles purified from the plasma samples of 8 patients with Stage IV melanoma (denoted as P1–P8). **f**, Immunoblots for PD-L1 in the exosomes purified from the plasma samples of 5 healthy donors and 5 patients with stage IV melanoma (left panel). Quantification of the levels of exosomal PD-L1 by western blot analysis (right panel). Results are expressed as the percentage of the mean value of healthy donors. **g**, Standard density gradient centrifugation analysis showing that circulating PD-L1 co-fractionated with exosome markers Hrs and TSG101 and melanoma-specific marker TYRP-2. Three (**c**, **d**) or two (**e**, **g**) experiments were repeated independently with similar results. Data represent mean ± s.d. (**a**, **b**, **f**). Statistical analyses were performed using two-sided unpaired *t*-test (**b**, **f**). For gel source data (**e**–**g**), see Supplementary Fig. 1.

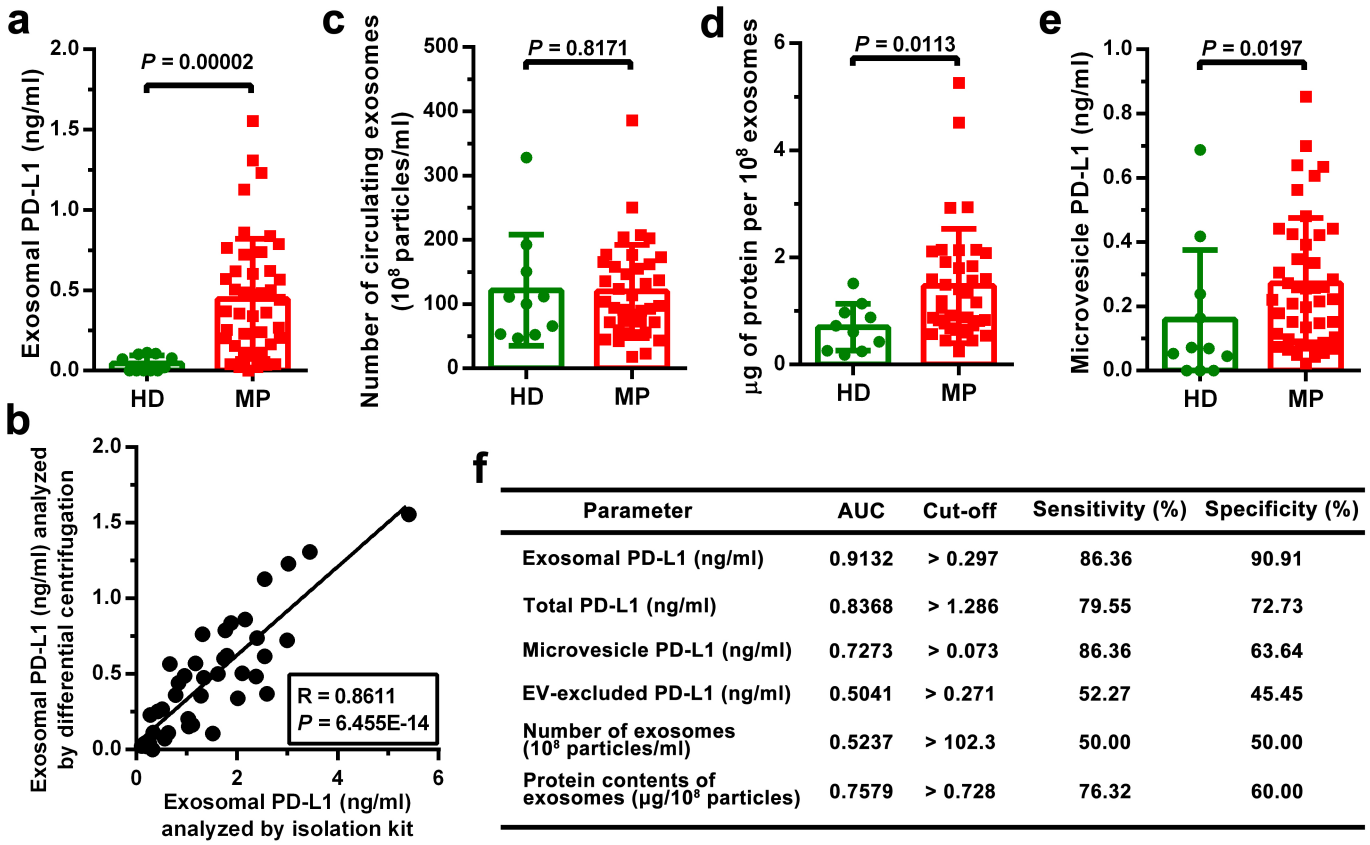

f

Parameter	AUC	Cut-off	Sensitivity (%)	Specificity (%)
Exosomal PD-L1 (ng/ml)	0.9132	> 0.297	86.36	90.91
Total PD-L1 (ng/ml)	0.8368	> 1.286	79.55	72.73
Microvesicle PD-L1 (ng/ml)	0.7273	> 0.073	86.36	63.64
EV-excluded PD-L1 (ng/ml)	0.5041	> 0.271	52.27	45.45
Number of exosomes (10^8 particles/ml)	0.5237	> 102.3	50.00	50.00
Protein contents of exosomes (μg/10^8 particles)	0.7579	> 0.728	76.32	60.00

Extended Data Fig. 3 | The number or bulk protein level of circulating exosomes shows no or modest difference between healthy donors and patients with metastatic melanoma. a, ELISA showing the level of PD-L1 on circulating exosomes purified from healthy donors (HD, $n = 11$) and melanoma patients (MP, $n = 44$). The exosomes were purified using differential centrifugation. **b**, Pearson correlation between the ELISA-detected levels of PD-L1 on circulating exosomes purified by differential centrifugation or using the commercial exosome isolation kit ($n = 44$). **c**, Comparison of the number of circulating exosomes between healthy donors ($n = 10$) and melanoma patients ($n = 38$). **d**, Comparison of the protein content of circulating exosomes between healthy donors ($n = 10$) and melanoma patients ($n = 38$). **e**, ELISA of the circulating level of microvesicle PD-L1 in healthy donors (HD, $n = 11$) and melanoma patients (MP, $n = 44$). **f**, Detailed data associated with the ROC curve analysis depicted in Fig. 2g. Data represent mean ± s.d. Statistical analyses are performed by two-sided unpaired *t*-test (**a**, **c**-**e**).

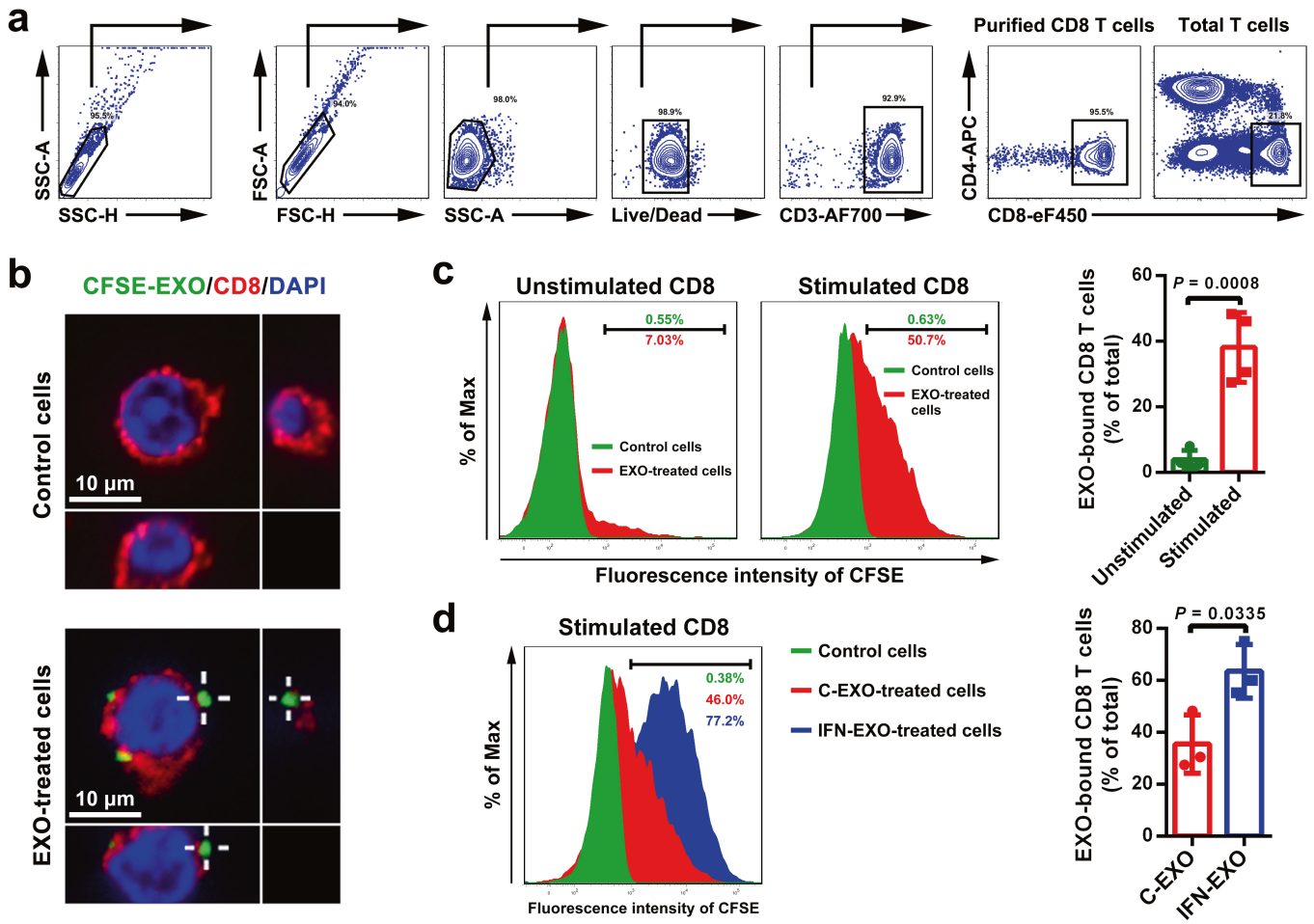

Extended Data Fig. 4 | Melanoma cell-derived exosomes bind to CD8 T cells on their surface. a, Representative contour plots showing the general gating strategy used to identify the purified CD8 T cells ($CD3^+CD8^+CD4^-$) from human peripheral blood. **b**, Confocal microscopy analysis of human peripheral CD8 T cells (stimulated with anti-CD3/CD28 antibodies) after incubation with CFSE-labelled WM9 cell-derived exosomes for 2 h. The experiments were repeated three times independently with similar results. **c**, Representative histogram of human peripheral CD8 T cells with or without anti-CD3/CD28 antibody stimulation after incubation with CFSE-labelled WM9 cell-derived exosomes for 2 h (left). The proportion of exosome-bound cells is shown (right). **d**, Representative histogram of human peripheral CD8 T cells (stimulated with anti-CD3/CD28 antibodies) after incubation with the same number of CFSE-labelled exosomes purified from control or IFN-γ-treated WM9 cells for 2 h (left panel). The proportion of EXO-bound cells is shown in the right panel. Data represent mean ± s.d. of four (**c**) or three (**d**) independent biological replicates. Statistical analyses are performed using two-sided unpaired *t*-test (**c**, **d**).

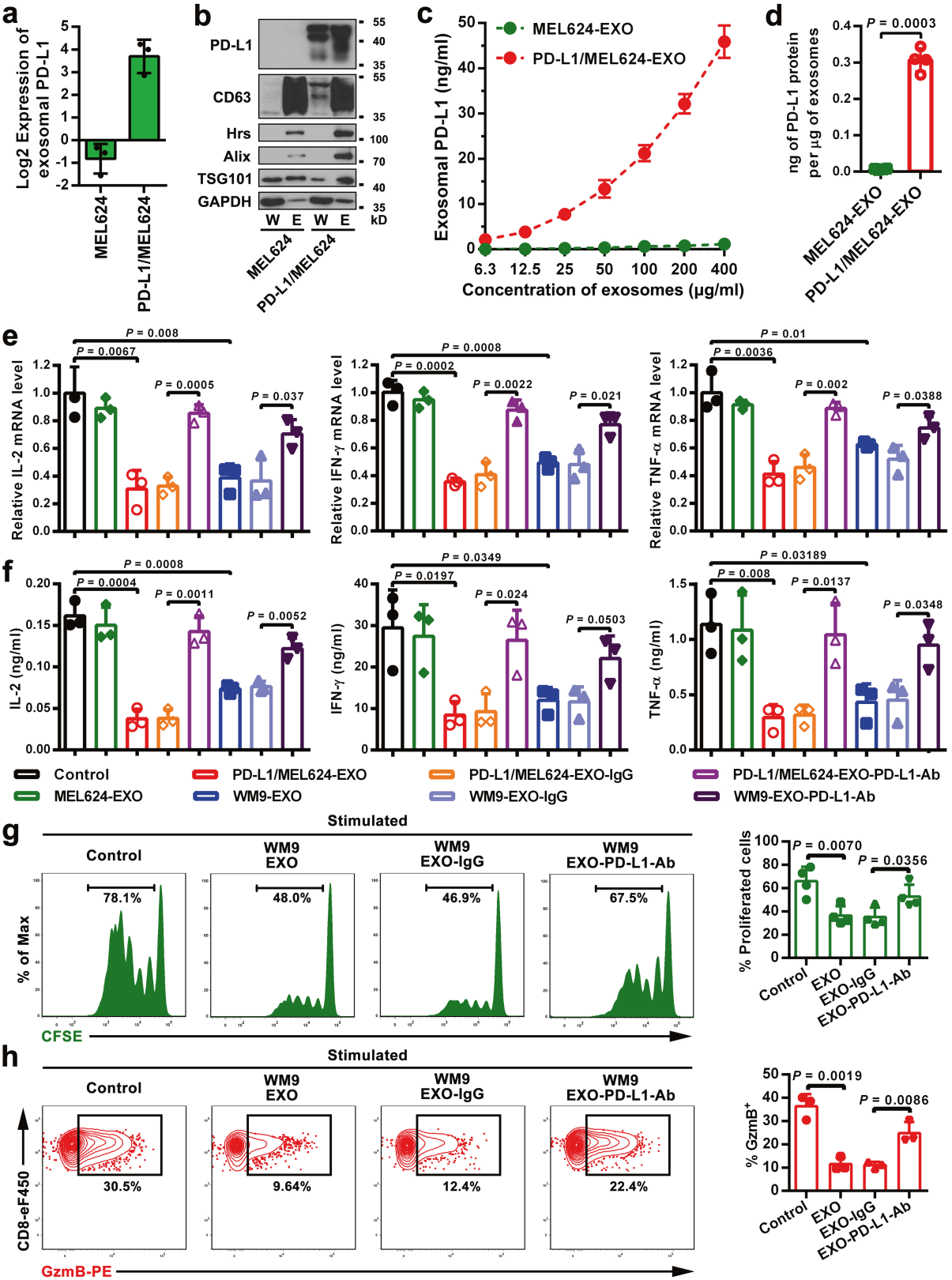

Extended Data Fig. 5 | See next page for caption.

Extended Data Fig. 5 | Functional inhibition of CD8 T cells by exosomal PD-L1. a, The log_2-transformed RPPA data showing the levels of PD-L1 in the exosomes secreted by control (MEL624) or PD-L1-expressing (PD-L1/MEL624) human melanoma MEL624 cells (Bottom). **b**, Immunoblots for PD-L1 in the whole cell lysate (W) or in the purified exosomes (E) from MEL624 or PD-L1/MEL624 cells. The same amount of protein was loaded in each lane. The experiments were repeated two times independently with similar results. For source data, see Supplementary Fig. 1. **c**, PD-L1 on the surface of exosomes secreted by MEL624 or PD-L1/MEL624 cells as determined by ELISA. **d**, Levels of PD-L1 on exosomes secreted by MEL624 or PD-L1/MEL624 cells, as measured by ELISA. **e**, qPCR analyses of IL-2, IFN-γ, and TNF in human peripheral CD8 T cells (stimulated with anti-CD3/CD28 antibodies) after treatment with MEL624 cell-derived exosomes, PD-L1/MEL624 cell-derived exosomes or WM9-cell-derived exosomes with or without blocking by IgG isotype or the anti-PD-L1 antibodies. The relative mRNA expression level was calculated as the ratio to the control cells. **f**, ELISA of IL-2, IFN-γ, and TNF in human peripheral CD8 T cells (stimulated with anti-CD3/CD28 antibodies) after treatment with MEL624 cell-derived exosomes, PD-L1/MEL624 cell-derived exosomes or WM9-cell-derived exosomes with or without blocking by IgG isotype or PD-L1 antibodies. **g**, Representative histogram of CFSE-labelled human peripheral CD8 T cells (stimulated with anti-CD3/CD28 antibodies) after treatment with WM9 cell-derived exosomes with or without antibody blocking (left). The proportion of cells with diluted CFSE dye is shown (right). **h**, Representative contour plots of human peripheral CD8 T cells (stimulated with anti-CD3/CD28 antibodies) examined for the expression of granzyme B (GzmB) after treatment with WM9 cell-derived exosomes with or without antibody blocking (left). The percentage of $GzmB^+$ CD8 T cells stimulated with anti-CD3/CD28 antibodies is shown at the right panel. Data represent mean ± s.d. of three (**a**, **c**, **e**, **f**, **h**) or four (**d**, **g**) independent biological replicates. Statistical analyses are performed using two-sided unpaired *t*-test (**d**–**h**).

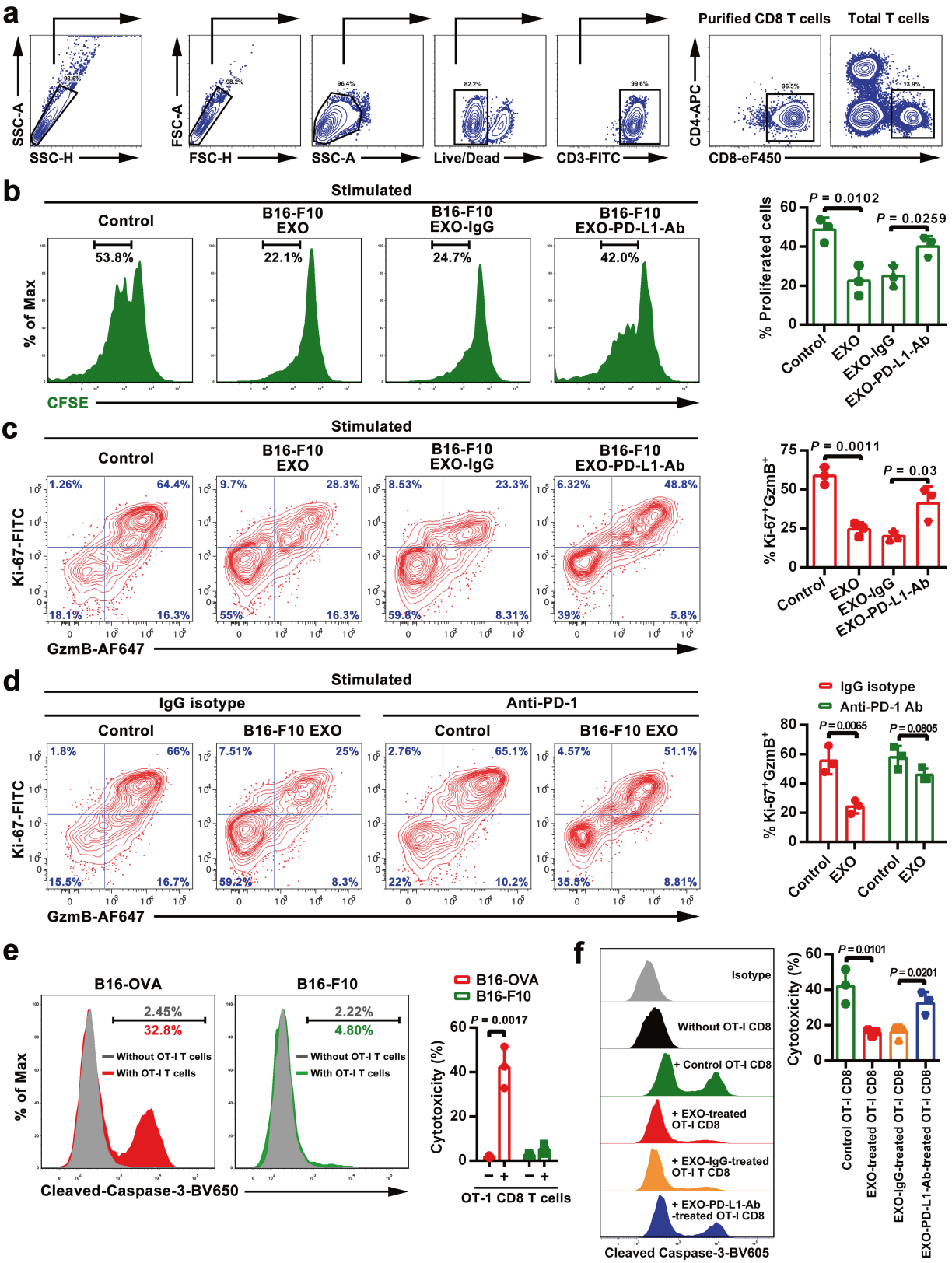

Extended Data Fig. 6 | See next page for caption.

Extended Data Fig. 6 | Exosomal PD-L1 secreted by mouse melanoma B16-F10 cells inhibits the proliferation and cytotoxicity of mouse splenic CD8 T cells. a, Representative contour plots showing the general gating strategy used to identify the purified CD8 T cells ($CD3^+CD8^+CD4^-$) from mouse splenocytes. **b**, Representative histogram of CFSE-labelled mouse splenic CD8 T cells (stimulated with anti-CD3/CD28 antibodies) after treatment with B16-F10 cell-derived exosomes with or without blocking by IgG isotype or the anti-PD-L1 antibodies (left). The proportion of cells with diluted CFSE dye is shown at the right panel. **c**, Representative contour plots of mouse splenic CD8 T cells (stimulated with anti-CD3/CD28 antibodies) examined for the expression of Ki-67 and granzyme B (GzmB) after treatment with B16-F10 cell-derived exosomes with or without blocking by IgG isotype or the anti-PD-L1 antibodies (left). The percentage of $Ki\text{-}67^+GzmB^+$ CD8 T cells stimulated with anti-CD3/CD28 antibodies is shown (right). **d**, Representative contour plots of mouse splenic CD8 T cells (stimulated with anti-CD3/CD28 antibodies) examined for the expression of Ki-67 and GzmB after treatment with B16-F10 cell-derived exosomes in the presence or absence of anti-PD-1 blocking antibodies (left). The percentage of $Ki\text{-}67^+GzmB^+$ CD8 T cells stimulated with anti-CD3/CD28 antibodies is shown at the right panel. **e**, OT-I CD8 T cell-meditated tumour cell killing assay was performed in B16-OVA cells with *PD-L1* knockdown, or B16-F10 cells with *PD-L1* knockdown (negative control). Apoptosis of tumour cells was evaluated by flow cytometric analysis of intracellular cleaved caspase-3 (left), and the relative cytotoxicity was calculated (right). **f**, OT-I CD8 T cells, activated by OVA-pulsed bone marrow-derived dendritic cells and treated with PBS (as a control), exosomes derived from B16-F10 cells with or without IgG isotype or PD-L1 antibody blocking, were co-cultured with *PD-L1* knockdown B16-OVA cells for 48 h. Tumour cell apoptosis was evaluated by flow cytometric analysis of intracellular cleaved caspase-3 (left), and the relative cytotoxicity was calculated (right). Data represent mean ± s.d. of three (**b**–**f**) independent biological replicates. Statistical analyses are performed using two-sided unpaired *t*-test (**b**–**f**).

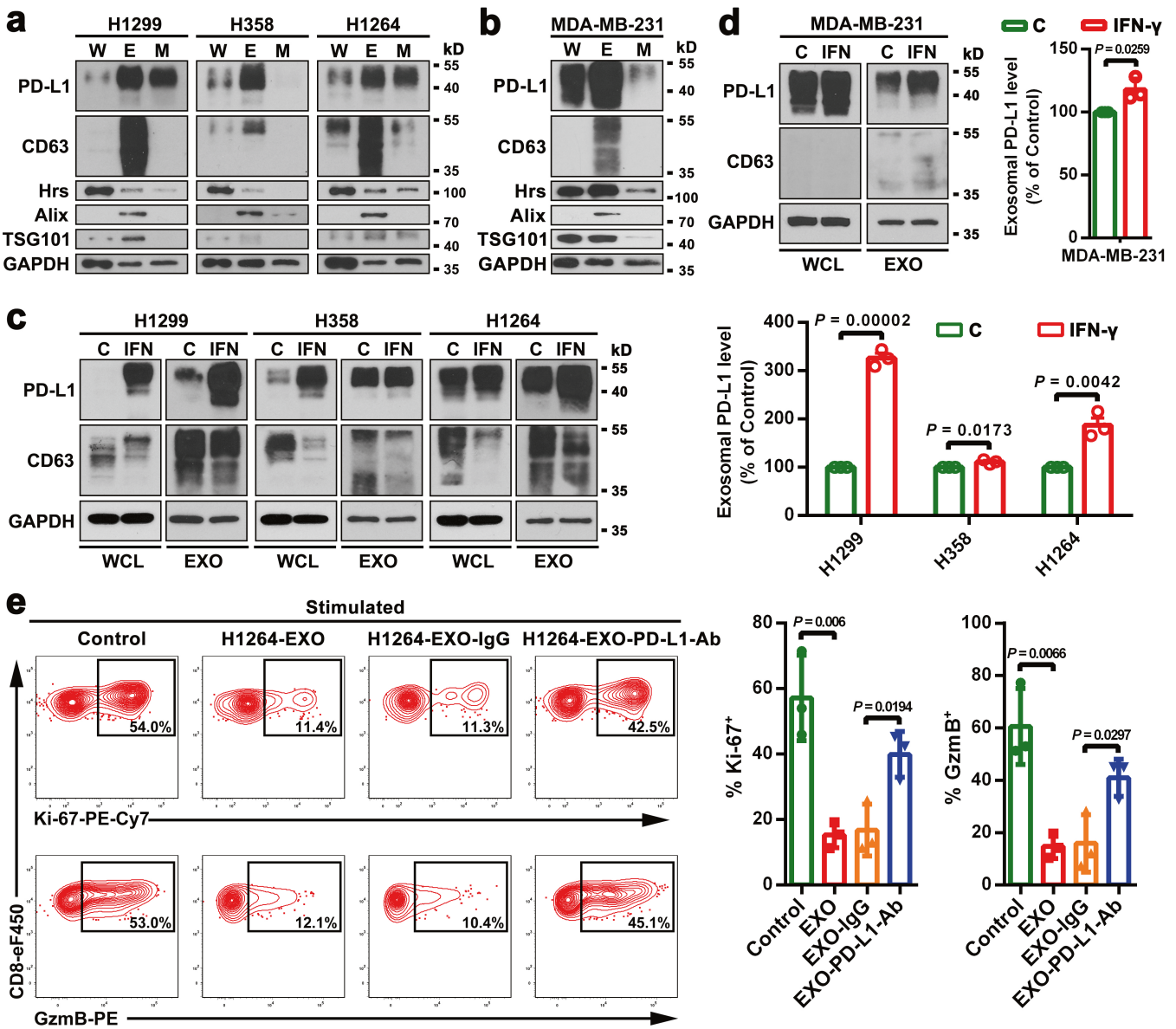

Extended Data Fig. 7 | Lung cancer and breast cancer cells release extracellular vesicles carrying PD-L1. a, Immunoblots for PD-L1 in the whole cell lysate (W), purified exosomes (E) or microvesicles (M) from different lung cancer cell lines. The same amounts of proteins were loaded for each fraction. **b**, Immunoblots for PD-L1 in the whole cell lysate, purified exosomes or microvesicles from the breast cancer cell line MDA-MB-231. The same amount of protein was loaded for each fraction. **c**, Immunoblots for PD-L1 in the whole cell lysate (WCL) or in the purified exosomes (EXO) from control (C) or IFN-γ-treated (IFN) lung cancer cells. The same amounts of exosome proteins from IFN-γ-treated and control cells were loaded (left). Quantification of the exosomal PD-L1 level determined by western blot analysis (right). **d**, Immunoblots for PD-L1 in the whole cell lysate or in the purified exosomes from control or IFN-γ-treated the breast cancer MDA-MB-231 cells. The same amounts of exosome proteins from IFN-γ-treated and control cells were loaded (left). Quantification of the exosomal PD-L1 level determined by western blot analysis (right). **e**, Representative contour plots of human peripheral CD8 T cells examined for the expression of Ki-67 and GzmB after treatment with H1264 cell-derived exosomes with or without blocking by IgG isotype or PD-L1 antibodies (left). The percentage of Ki-67$^+$ or GzmB$^+$ CD8 T cells is shown (right). The experiments were repeated twice independently with similar results (**a**, **b**). Data represent mean ± s.d. of three (**c**–**e**) independent biological replicates. Statistical analyses are performed using two-sided unpaired *t*-test (**c**–**e**). For source data (**a**–**d**), see Supplementary Fig. 1.

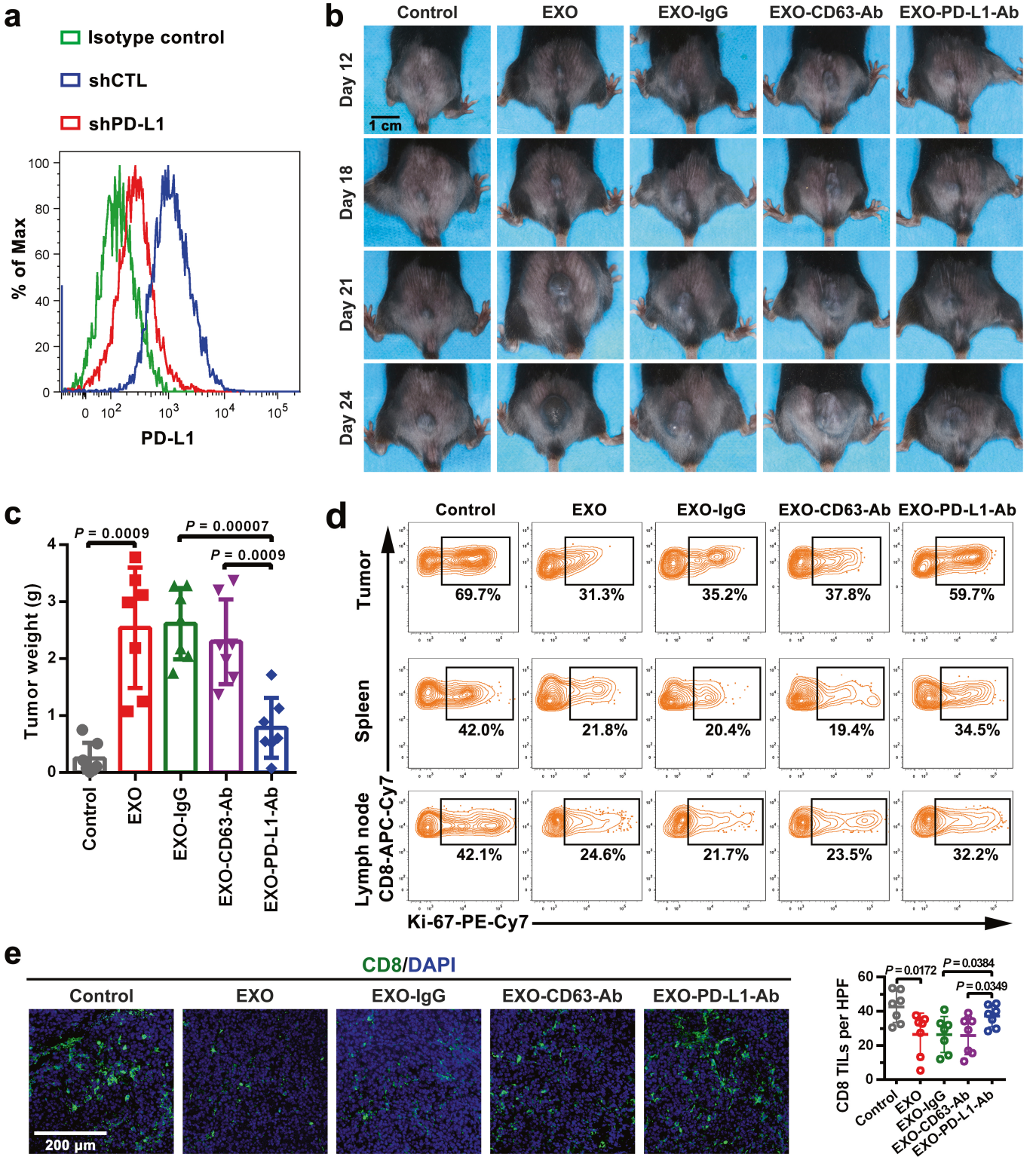

Extended Data Fig. 8 | Exosomal PD-L1 facilitates melanoma growth in vivo. a, Representative flow cytometric histograms of B16-F10 cells examined for the expression of PD-L1 with or without *PD-L1* knockdown. B16-F10 cells were stably depleted of *PD-L1* using lentiviral shRNA against *PD-L1* (shPD-L1) or the scrambled control shRNA (shCTL). The experiment was repeated twice independently with similar results. **b**, Representative images showing the growth of *PD-L1* knockdown B16-F10 tumours in C57BL/6 mice after indicated treatments. Experiments were performed using 7 mice for each group. **c**, The weights of *PD-L1* knockdown B16-F10 tumours from C57BL/6 mice with indicated treatments ($n = 7$ mice per group). Data represent mean ± s.d. **d**, Representative contour plot of CD8 TILs or splenic or lymph node CD8 T cells examined for the expression of Ki-67 after indicated treatments. Experiments were performed using 7 mice for each group. See Fig. 3c for quantification data. **e**, Representative immunofluorescence images of CD8 TILs in tumour tissues (left). The number of CD8 TILs for each mouse ($n = 7$ mice per group) were quantified from 5 high-power fields (HPF) (right). Statistical analysis is performed using two-sided unpaired *t*-test (**c**, **e**).

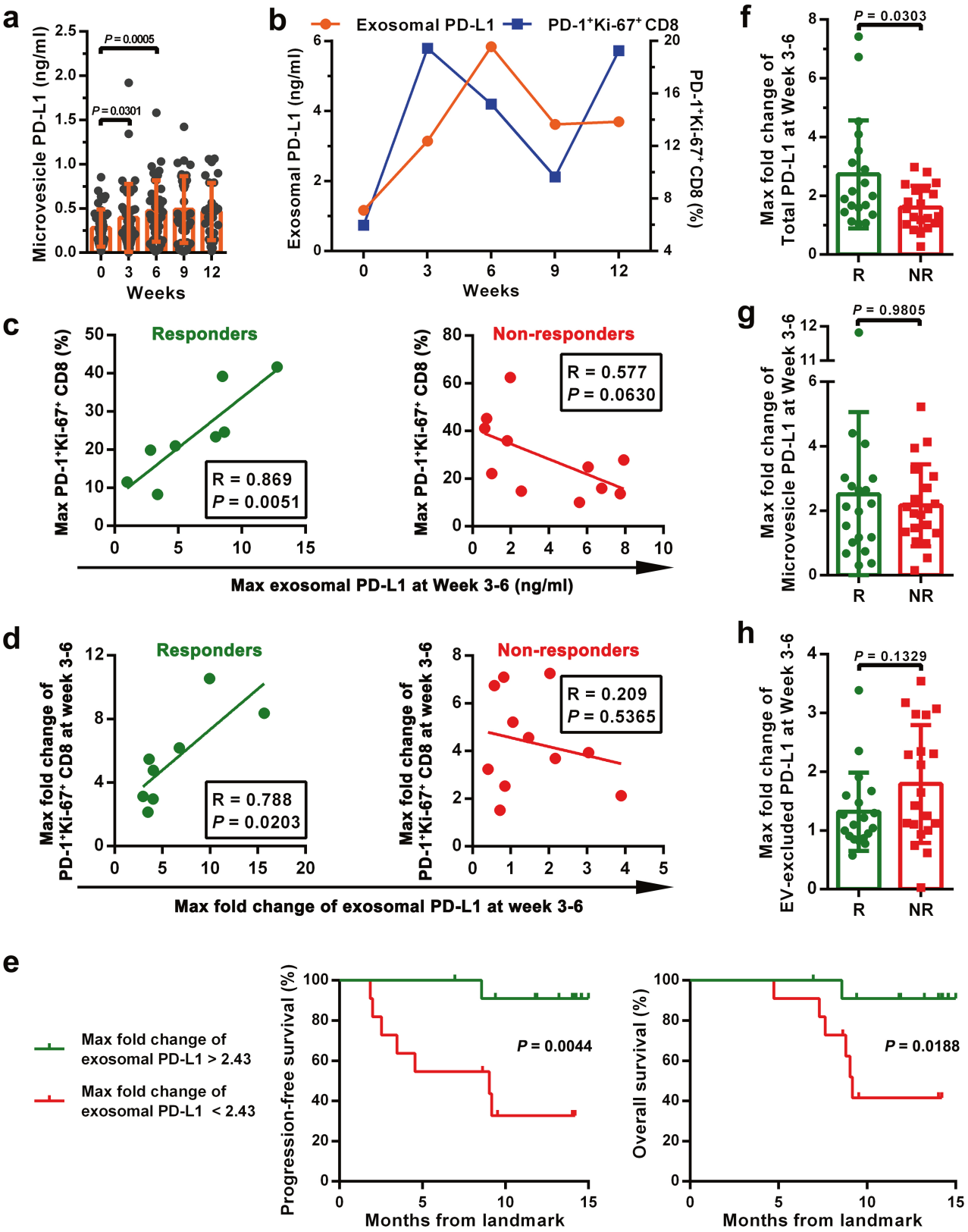

Extended Data Fig. 9 | See next page for caption.

Extended Data Fig. 9 | The level of circulating exosomal PD-L1 distinguishes clinical responders to pembrolizumab treatment from non-responders. a, The levels of PD-L1 on circulating microvesicles at serial time points pre- and on-treatment ($n = 39$). **b**, The frequency of PD-1$^+$ Ki-67$^+$ CD8 T cells and the level of circulating exosomal PD-L1 in clinical responders at serial time points pre- and on-treatment ($n = 8$). **c**, Pearson correlation of the maximum level of circulating exosomal PD-L1 at week 3–6 to the maximum frequency of PD-1$^+$Ki-67$^+$ CD8 T cells at week 3–6 in clinical responders ($n = 8$) and non-responders ($n = 11$). **d**, Pearson correlation of the maximum fold change of circulating exosomal PD-L1 level at week 3–6 to the maximum fold change of PD-1$^+$Ki-67$^+$ CD8 T cells at week 3–6 in clinical responders ($n = 8$) and non-responders ($n = 11$). **e**, Kaplan–Meier progression-free and overall survival of patients with high ($n = 11$) and low ($n = 12$) fold changes of circulating exosomal PD-L1 at 3–6 weeks. **f**, Comparison of the maximum fold change of total circulating PD-L1 at week 3–6 between the clinical responders and non-responders. R, responders, $n = 19$; NR, non-responders, $n = 20$. **g**, Comparison of the maximum fold change of circulating microvesicle PD-L1 at week 3–6 between the clinical responders ($n = 19$) and non-responders ($n = 20$). **h**, Comparison of the maximum fold change of extracellular-excluded PD-L1 at week 3–6 between the clinical responders ($n = 19$) and non-responders ($n = 20$). Data represent mean ± s.d. Statistical analyses were performed using two-sided paired *t*-test (**a**), log-rank test (**e**), or two-sided unpaired *t*-test (**f**–**h**).

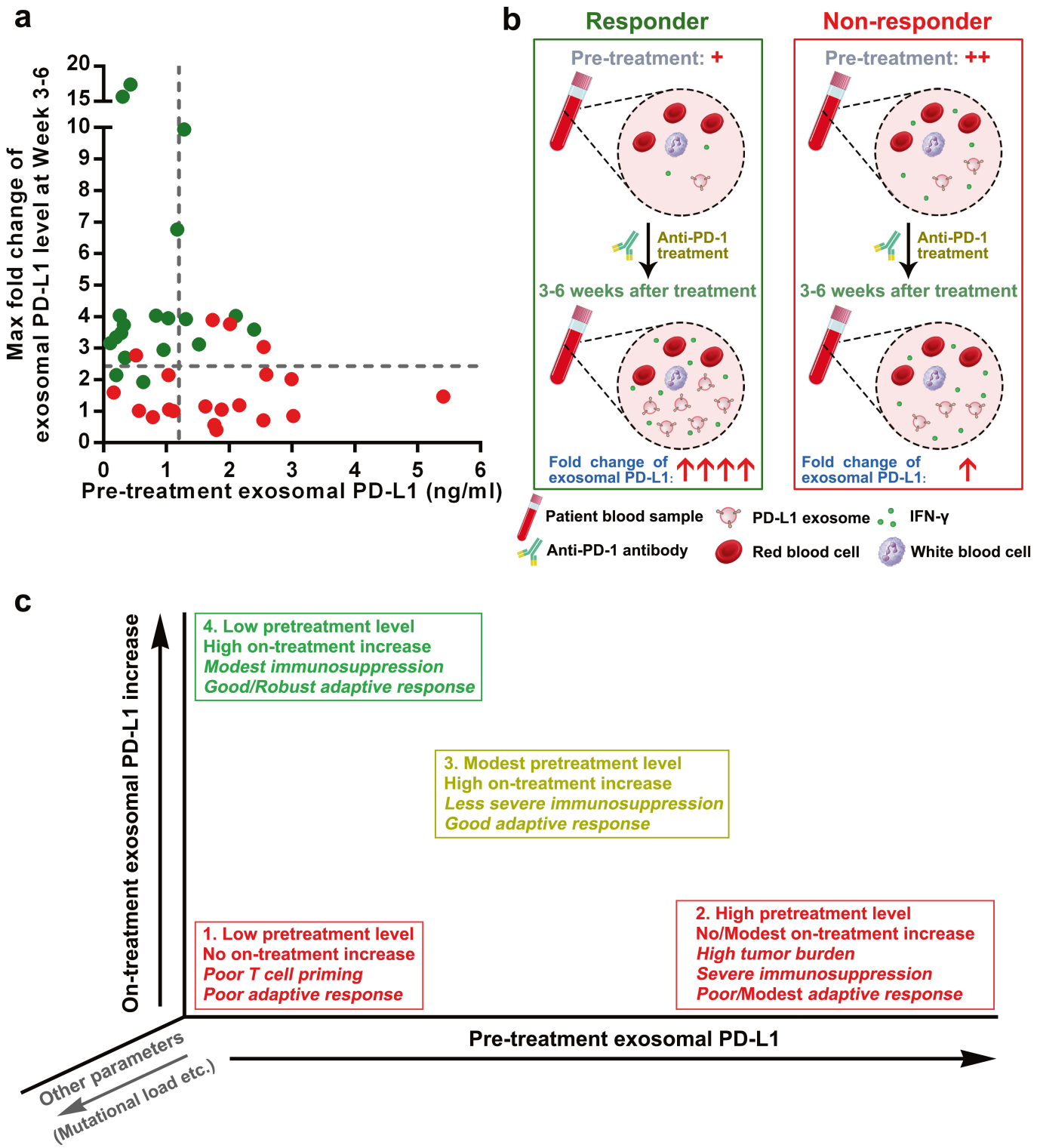

Extended Data Fig. 10 | Circulating exosomal PD-L1 is a potential rationale-based and clinically accessible predictor for clinical outcomes of anti-PD-1 therapy. a, Tracking the levels of circulating exosomal PD-L1 before and during anti-PD-1 treatment may stratify responders to anti-PD-1 therapy (green) from non-responders (red) as early as 3–6 weeks into the treatment. **b**, Potential application of circulating exosomal PD-L1 to predict patients' response to anti-PD-1 therapy. The pre-treatment level of circulating exosomal PD-L1 is lower in metastatic melanoma patients with clinical response to anti-PD-1 therapy. After 3–6 weeks of anti-PD-1 treatment, the level of circulating exosomal PD-L1 increases significantly in clinical responders but not in non-responders. **c**, Tracking both the pre-treatment and on-treatment levels of circulating exosomal PD-L1 may help identify the possible reasons for success (green) or failure (red) of the therapy.

nature research

Corresponding author(s): Wei Guo and Xiaowei Xu

Reporting Summary

Nature Research wishes to improve the reproducibility of the work that we publish. This form provides structure for consistency and transparency in reporting. For further information on Nature Research policies, see Authors & Referees and the Editorial Policy Checklist.

Statistical parameters

When statistical analyses are reported, confirm that the following items are present in the relevant location (e.g. figure legend, table legend, main text, or Methods section).

n/a	Confirmed	
☐	☒	The exact sample size (*n*) for each experimental group/condition, given as a discrete number and unit of measurement
☐	☒	An indication of whether measurements were taken from distinct samples or whether the same sample was measured repeatedly
☐	☒	The statistical test(s) used AND whether they are one- or two-sided *Only common tests should be described solely by name; describe more complex techniques in the Methods section.*
☐	☒	A description of all covariates tested
☐	☒	A description of any assumptions or corrections, such as tests of normality and adjustment for multiple comparisons
☐	☒	A full description of the statistics including central tendency (e.g. means) or other basic estimates (e.g. regression coefficient) AND variation (e.g. standard deviation) or associated estimates of uncertainty (e.g. confidence intervals)
☐	☒	For null hypothesis testing, the test statistic (e.g. *F*, *t*, *r*) with confidence intervals, effect sizes, degrees of freedom and *P* value noted *Give P values as exact values whenever suitable.*
☒	☐	For Bayesian analysis, information on the choice of priors and Markov chain Monte Carlo settings
☒	☐	For hierarchical and complex designs, identification of the appropriate level for tests and full reporting of outcomes
☐	☒	Estimates of effect sizes (e.g. Cohen's *d*, Pearson's *r*), indicating how they were calculated
☐	☒	Clearly defined error bars *State explicitly what error bars represent (e.g. SD, SE, CI)*

Our web collection on statistics for biologists may be useful.

Software and code

Policy information about availability of computer code

Data collection	BD FACSDiva V8.0.1, NTA 3.2 software, KC4 V3.0 Data reduction software, Nikon's NIS Elements V4.0
Data analysis	GraphPad Prism V6.0.1, FlowJo 10.4.2, ImageJ 1.52a, Software R 2.14. The package binaries of SuperCurve and SuperCurveGUI used for the analysis of RPPA data are available in R-Forge (https://r-forge.r-project.org/R/?group_id=1899).

For manuscripts utilizing custom algorithms or software that are central to the research but not yet described in published literature, software must be made available to editors/reviewers upon request. We strongly encourage code deposition in a community repository (e.g. GitHub). See the Nature Research guidelines for submitting code & software for further information.

Data

Policy information about availability of data

All manuscripts must include a data availability statement. This statement should provide the following information, where applicable:

- Accession codes, unique identifiers, or web links for publicly available datasets
- A list of figures that have associated raw data
- A description of any restrictions on data availability

The authors declare that the data supporting the findings of this study are available within the paper and its supplementary information files.

Field-specific reporting

Please select the best fit for your research. If you are not sure, read the appropriate sections before making your selection.

☒ Life sciences ☐ Behavioural & social sciences

For a reference copy of the document with all sections, see nature.com/authors/policies/ReportingSummary-flat.pdf

Life sciences

Study design

All studies must disclose on these points even when the disclosure is negative.

Sample size	Samples size for each experiment is indicated in the figures or corresponding figure legends. The sample size of sufficient statistical power in mice study was chosen based on previous experience in the lab or previously published studies using similar analyses (PMIDs, 28953887, 27912060, 26493961, 27866850).
Data exclusions	No data were excluded from the analyses.
Replication	All replicates reported in the manuscript are biological replicates. All the statistics reported in the manuscript are based on at least 3 biologically independent replicates. All attempts to replicate the experiments were successful.
Randomization	Mice were allocated randomly to each treatment group.
Blinding	The assessment of clinical responses for patients was performed independently in a double-blind fashion. For mice studies, the experiments were performed in a blinded fashion when possible. Downstream analyses of mouse samples (immunofluorescence staining, flow cytometry and ELISA) were performed in a blinded fashion, which means that people performing the assays were not aware of the treatment groups until the data analyses were completed.

Materials & experimental systems

Policy information about availability of materials

n/a	Involved in the study
☐	☒ Unique materials
☐	☒ Antibodies
☐	☒ Eukaryotic cell lines
☐	☒ Research animals
☐	☒ Human research participants

Unique materials

Obtaining unique materials	shRNA against human Hrs (GCATGAAGAGTAACCACAGC), shRNA against human Rab27a (CAGGAGAGGTTTCGTAGCTA) and mouse melanoma B16 cells stably expressing chicken OVA (B16-OVA) were obtained under Material Transfer Agreements. Cell lines including the control and PD-L1-overexpressing human melanoma MEL624 cells, human melanoma WM1552C, WM35, WM793, WM902B, WM9 and WM164 cells, human melanoma UACC-903 cells, PD-L1 antibody (clone 5H1-A3) are available from the authors on reasonable request. All other materials are commercially available.

Antibodies

Antibodies used	The following primary antibodies were used for western blotting. They are listed as antigen first, followed by dilution, host, supplier, catalog number and clone/lot number as applicable. 1) Anti-human PD-L1, 1:500, Rabbit, Cell Signaling Technology, #13684, clone E1L3N; 2) Anti-Hrs, 1:2000, Rabbit, Cell Signaling Technology, #15087S, clone D7T5N; 3) Anti-Alix, 1:1000, Mouse, Cell Signaling Technology, #2171S, clone 3A9; 4) Anti-human CD63, 1:1000, Rabbit, Abcam, ab68418; 5) Anti-TSG101, 1:1000, Rabbit, Abcam, ab125011, clone EPR7130(B); 6) Anti-TYRP1, 1:500, Rabbit, Abcam, ab83774; 7) Anti-TYRP2, 1:500, Rabbit, Thermo Fisher Scientific, PA5-36485; 8) Anti-Rab27a, 1:500, Goat, SICGEN, AB0045; 9) Anti-GAPDH, 1:4000, Rabbit, Cell Siganling Technology, #5174S, clone D16H11; 10) Anti-Actin, 1:5000, Rabbit, Cell Signaling Technology, #3700S, clone 8H10D10; 11) Anti-Flag, 1:2000, Mouse, Sigma, F1804, clone M2;

The following primary antibodies were used for immunofluorescence. They are listed as antigen first, followed by dilution, host, supplier, catalog number and clone/lot number as applicable.
1) Anti-human PD-L1, 1:200, Mouse, Lab of Haidong Dong, clone 5H1;
2) Anti-human PD-L1, 1:200, Rabbit, Cell Signaling Technology, #86744, clone D8T4X;
3) Anti-human CD63, 1:100, Mouse, Abcam, ab8219, clone MEM-259;
4) Anti-Hrs, 1:200, Rabbit, Cell Signaling Technology, #15087S, clone D7T5N;
5) Anti-Human CD8a, 1:200, BioLegend, 13983, clone C8/144B;
6) Anti-mouse CD8a, 1:400, Cell Signaling Technology, #98941T, clone D4W2Z;

The following primary antibodies were used for flow cytometry. They are listed as antigen first, followed by dilution, host, supplier, catalog number and clone/lot number as applicable.
1) Anti-human PD-L1 (PE), 1:40, Mouse, BioLegend, 329706, clone 29E.2A3;
2) Anti-human PD-L1 (FITC), 1:20, Mouse, BD Biosciences, 558065, clone MIH1;
3) Anti-human CD3 (Alexa Fluor 700), 1:100, Mouse, BioLegend, 317340, clone OKT3;
4) Anti-human CD8a (eFluor450), 1:100, Mouse, eBiosciences, 48-0088-42, clone RPA-T8;
5) Anti-human CD4 (APC), 1:100, Mouse, BioLegend, 317416, clone OKT4;
6) Anti-human PD-1 (FITC), 1:20, Mouse, BioLegend, 329904, clone EH12.2H7;
7) Anti-human Ki67 (PE-Cy7), 1:100, Mouse, BD Biosciences, 561283, clone B56;
8) Anti-human Granzyme B (PE), 1:100, Mouse, Life Technologies, GRB04, clone GB11;
9) Anti-mouse PD-1 (PE-Cy7), 1:20, Rat, BioLegend, 109110, clone RMP1-30;
10) Anti-mouse Ki67 (Alexa Fluor 700), 1:20, Rat, BioLegend, 652420, clone 16A8;
11) Anti-mouse Ki67 (FITC), 1:20, Rat, BioLegend, 652410, clone 16A8;
12) Anti-mouse Ki67 (PE-Cy7), 1:20, Rat, BioLegend, 652426, clone 16A8;
13) Anti-mouse Granzyme B (PE), 1:20, Rat, eBioscience, 12-8898-82, clone NGZB;
14) Anti-mouse Granzyme B (Alexa Fluor 647), 1:20, Rat, BioLegend, 515406, clone GB11;
15) Anti-mouse CD3 (FITC), 1:100, Rat, BioLegend, 100204, clone 17A2;
16) Anti-mouse CD8a (eFluor 450), 1:100, Rat, eBioscience, 48-0081-82, clone 53-6.7;
17) Anti-mouse CD8a (APC-Cy7), 1:100, Rat, BioLegend, 100714, clone 53-6.7;
18) Anti-active caspase-3 (BV650), 1:20, Rabbit, BD Biosciences, 564096, clone C92-605.

The following primary antibodies were used for blocking. They are listed as antigen first, followed by dilution, host, supplier, catalog number and clone/lot number as applicable.
1) Anti-human PD-L1, 1:50, Mouse, Lab of Haidong Dong, clone 5H1;
2) Mouse IgG isotype, 1:100, Mouse, BioLegend, 401404, clone MG1-45;
3) Anti-mouse PD-1, 1:100, Rat, BioLegend, 135203, clone 29F.1A12;
4) Rat IgG isotype, 1:100, Rat, BioLegend, 400543, clone RTK2758;
5) Anti-mouse PD-L1, 1:600, Rat, Bio X Cell, BE0101, clone 10F.9G2;
6) Rat IgG2b isotype control, 1:600, Rat, Bio X Cell, BE0090, clone LTF-2.

The following primary antibodies were used for ELISA. They are listed as antigen first, followed by dilution, host, supplier, catalog number and clone/lot number as applicable.
1) For capture, anti-human PD-L1, 1:200, Mouse, Lab of Haidong Dong, clone 5H1;
2) For detection, anti-human PD-L1 (biotin), 1:500, Mouse, eBioscience, 13-5983-82, clone MIH1.

Validation

The mouse anti-human PD-L1 antibody was generated and validated in Dr. Haidong Dong's Lab (Frigola, et al., Clin. Cancer Res., 2011;17:1915-23). All other antibodies were purchased from commercial companies, and validated by the data sheets of the manufacturer or citations listed below.
1) Anti-human PD-L1, validated with melanoma cells in Natale et al., 2018, eLife, PMID 29336307;
2) Anti-Hrs, validated by western blot analysis of extracts from various cell lines (https://www.cellsignal.com/products/primary-antibodies/hrs-d7t5n-rabbit-mab/15087?site-search-type=Products&N=4294956287&Ntt=15087s&fromPage=plp&_requestid=1487436) ;
3) Anti-Alix, validated with exosomes derived from bladder carcinoma cells in Ostenfeld et al., 2014, Cancer Res, PMID 25261234;
4) Anti-human CD63, validated by western blot analysis of extracts of human heptocellular liver carcinoma cell line (http://www.abcam.com/cd63-antibody-ab68418.html);
5) Anti-TSG101, validated with EVs derived from B16F10 and mouse CD8 T cells in Seo et al., 2018, Nat Commun, PMID 29382847;
6) Anti-TYRP1, validated with western blot analysis of extracts of 721_B cell (http://www.abcam.com/TRP1-antibody-ab83774.html#description_images_1);
7) Anti-TYRP2, validated with western blot analysis of extracts of HEK293T cell (https://www.thermofisher.com/antibody/product/DCT-Antibody-Polyclonal/PA5-36485);
8) Anti-Rab27a, validated with western blot analysis of extracts of mouse pituitary tumor cell AtT-20 (http://www.sicgen.pt/product/rab27a-polyclonal-antibody_1_32);
9) Anti-GAPDH, validated with western blot analysis of extracts of various cell lines (https://www.cellsignal.com/products/primary-antibodies/gapdh-d16h11-xp-rabbit-mab/5174?site-search-type=Products&N=4294956287&Ntt=5174s&fromPage=plp&_requestid=1488597);
10) Anti-Actin, validated with western blot analysis of extracts of various cell lines (https://www.cellsignal.com/products/primary-antibodies/b-actin-8h10d10-mouse-mab/3700?site-search-type=Products&N=4294956287&Ntt=8h10d10&fromPage=plp);
11) Anti-Flag, validated with Flag transfected cells in Hirata et al., 2018, Nat Commun, PMID 25254944;

The following primary antibodies were used for immunofluorescence.
1) Anti-human PD-L1, validated with human intestinal mucosa in Takanori et al., 2003, J immunol, PMID 14530338;
2) Anti-human PD-L1, validated with immunofluorescence analysis of various cell lines (https://www.cellsignal.com/products/primary-antibodies/pd-l1-extracellular-domain-specific-d8t4x-rabbit-mab/86744) ;

3) Anti-human CD63, validated with immunofluorescence analysis of human fibrosarcoma cells (http://www.abcam.com/cd63-antibody-mem-259-ab8219.html);
4) Anti-Hrs, validated with immunofluorescence analysis of HeLa cells (https://www.cellsignal.com/products/primary-antibodies/hrs-d7t5n-rabbit-mab/15087?site-search-type=Products&N=4294956287&Ntt=15087s&fromPage=plp&_requestid=1489630);
5) Anti-human CD8a, validated with immunofluorescence analysis of human paraffin-embedded tonsil tissue (https://www.biolegend.com/en-us/products/purified-anti-human-cd8a-antibody-13983);
6) Anti-mouse CD8a, validated with immunofluorescence analysis of paraffin-embedded mouse LL2 syngeneic tumor tissue (https://www.cellsignal.com/products/primary-antibodies/cd8a-d4w2z-xp-rabbit-mab-mouse-specific/98941?site-search-type=Products&N=4294956287&Ntt=cd8a&fromPage=plp);

The following primary antibodies were used for flow cytometry.
1) Anti-human PD-L1 (PE), validated with FC of PHA-stimulated human peripheral blood lymphocytes (https://www.biolegend.com/en-us/products/pe-anti-human-cd274-b7-h1--pd-l1-antibody-4375);
2) Anti-human PD-L1 (FITC), validated with human breast cancer cell lines in Latchman et al., 2001, Nat Immunol, PMID 11224527;
3) Anti-human CD3 (Alexa Fluor 700), validated with FC of normal human peripheral blood cells (https://www.biolegend.com/en-us/products/alexa-fluor-700-anti-human-cd3-antibody-9625);
4) Anti-human CD8a (eFluor450), validated with FC of normal human peripheral blood cells (https://www.thermofisher.com/antibody/product/CD8a-Antibody-clone-RPA-T8-Monoclonal/48-0088-42);
5) Anti-human CD4 (APC), validated with FC of normal human peripheral blood cells (https://www.biolegend.com/en-us/products/apc-anti-human-cd4-antibody-3657);
6) Anti-human PD-1 (FITC), validated with FC of PHA-stimulated human peripheral blood lymphocytes (https://www.biolegend.com/en-us/products/fitc-anti-human-cd279-pd-1-antibody-4411);
7) Anti-human Ki67 (PE-Cy7), validated with FC of proliferating Molt-4 cells and noncycling PBMC (http://www.bdbiosciences.com/us/applications/research/intracellular-flow/intracellular-antibodies-and-isotype-controls/anti-human-antibodies/pe-cy7-mouse-anti-ki-67-b56/p/561283);
8) Anti-human Granzyme B (PE), validated with CD8+ T cells in Romano et al., 2015, J Immunol, PMID 26371247;
9) Anti-mouse PD-1 (PE-Cy7), validated with FC of Con A-stimulated Balb/c mouse splenocytes (https://www.biolegend.com/en-us/products/pe-cy7-anti-mouse-cd279-pd-1-antibody-3612);
10) Anti-mouse Ki67 (Alexa Fluor 700), validated with FC of IL-2-stimulated C57BL/6 mouse splenocytes (https://www.biolegend.com/en-us/products/alexa-fluor-700-anti-mouse-ki-67-antibody-10366);
11) Anti-mouse Ki67 (FITC), validated with FC of Con A-stimulated (3 days) BALB/c mouse splenocytes (https://www.biolegend.com/en-us/products/fitc-anti-mouse-ki-67-antibody-8573);
12) Anti-mouse Ki67 (PE-Cy7), validated with FC of Con A+IL-2 stimulated (3 days) C57BL/6 mouse splenocytes (https://www.biolegend.com/en-us/products/pe-cy7-anti-mouse-ki-67-antibody-13821);
13) Anti-mouse Granzyme B (PE), validated with CD8+ T cells in Klein-Hessling et al., 2017, Nat Commun, PMID 28894104;
14) Anti-mouse Granzyme B (Alexa Fluor 647), validated with FC of human peripheral blood lymphocytes were surface stained with CD8 PE (https://www.biolegend.com/en-us/products/alexa-fluor-647-anti-human-mouse-granzyme-b-antibody-6067);
15) Anti-mouse CD3 (FITC), validated with FC of C57BL/6 splenocytes (https://www.biolegend.com/en-us/products/fitc-anti-mouse-cd3-antibody-45);
16) Anti-mouse CD8a (eFluor 450), validated with FC of mouse CD8+ T cells in Pishesha et al., 2017, Proc Natl Acad Sci U S A, PMID 28270614;
17) Anti-mouse CD8a (APC-Cy7), validated with FC of C57BL/6 mouse splenocytes (https://www.biolegend.com/en-us/products/apc-cy7-anti-mouse-cd8a-antibody-2269);
18) Anti-active caspase-3 (BV650), validated with FC of apoptotic Jurkat cells (http://www.bdbiosciences.com/us/reagents/research/antibodies-buffers/cell-biology-reagents/cell-biology-antibodies/bv650-rabbit-anti--active-caspase-3-c92-605/p/564096).

The following primary antibodies were used for blocking.
1) Anti-human PD-L1, validated with human T cell lymphoma cell line in Liu et al., 2016, Sci Rep, PMID 27824138;
2) Mouse IgG isotype, validated with primary mouse macrophages in Prasad et al., 2016, J immunol, PMID 27647836;
3) Anti-mouse PD-1, validated with mouse CD8+ T cells in vivo in Barber et al., 2006, Nature, PMID 16382236;
4) Rat IgG isotype, validated with mice in vivo in Mbofung et al., 2017, Nat Commun, PMID 28878208;
5) Anti-mouse PD-L1, validated in Liu et al., 2016, Sci Rep, PMID 27824138;
6) Rat IgG2b isotype control, validated in Aloulou et al., 2016, Nat Commun, PMID 26818004.

The following primary antibodies were used for ELISA.
1) For capture, anti-human PD-L1, validated in the Lab of Haidong Dong;
2) For detection, anti-human PD-L1 (biotin), validated with normal human peripheral blood cells (https://www.thermofisher.com/antibody/product/CD274-PD-L1-B7-H1-Antibody-clone-MIH1-Monoclonal/13-5983-82).

Eukaryotic cell lines

Policy information about cell lines

Cell line source(s)	The A375 human melanoma and B16-F10 mouse melanoma cells were purchased from ATCC. The control and PD-L1-overexpressing human melanoma MEL624 cells were provided by Dr. Haidong Dong (Mayo Clinic). Mouse melanoma B16 cells stably expressing chicken OVA (B16-OVA) were provided by Hildegund C.J. Ertl (The Wistar Institute). The UACC-903 human melanoma cells were provided by Dr. Marianne Powell (Stanford University). The melanoma cell lines WM1552C, WM35, WM793, WM902B, WM9 and WM164 presented in this study were established in Dr. Meenhard Herlyn's lab (The Wistar Institute).
Authentication	All cell lines presented in this study were authenticated by DNA fingerprinting.

Mycoplasma contamination	All the cell lines presented in this study were tested for mycoplasma contamination and they were free of mycoplasma contamination.
Commonly misidentified lines (See ICLAC register)	No commonly misidentified cell lines were used.

Research animals

Policy information about studies involving animals; ARRIVE guidelines recommended for reporting animal research

Animals/animal-derived materials	Eight-week-old female athymic nude mice were used to establish melanoma xenograft. Six-to-eight-week-old, female and male, immunocompetent C57BL/6 mice were used to establish mouse melanoma model.

Human research participants

Policy information about studies involving human research participants

Population characteristics	Plasma samples of 44 individual patients with metastatic melanoma: 25 male, 19 female; age range 29-89 years, median 64 years; 10 AJCC stage III, 34 AJCC stage IV. Participants of irRECIST evaluated response: 13 complete response (CR), 8 partial response (PR), 7 stable disease (SD), 16 progressive disease (PD). Plasma samples of 11 healthy donors: 7 male, 4 female; age range 22-71 years, median 48 years.

Method-specific reporting

n/a	Involved in the study
☒	☐ ChIP-seq
☐	☒ Flow cytometry
☒	☐ Magnetic resonance imaging

Flow Cytometry

Plots

Confirm that:

☒ The axis labels state the marker and fluorochrome used (e.g. CD4-FITC).

☒ The axis scales are clearly visible. Include numbers along axes only for bottom left plot of group (a 'group' is an analysis of identical markers).

☒ All plots are contour plots with outliers or pseudocolor plots.

☒ A numerical value for number of cells or percentage (with statistics) is provided.

Methodology

Sample preparation	For characterization of exosomal PD-L1, purified exosomes were incubated with CD63-coated magnetic beads in 100 µl of isolation buffer (PBS with 0.1% BSA) overnight at 4 °C with mixing. Then, the exosome-bound beads were washed twice with isolation buffer and incubated with fluorophore-labeled anti-PD-L1 antibodies for 60 min at 4 °C . For analyzing the level of cleaved-Caspase-3, cells were collected and washed, and then fixed and permeabilized with the FOXP3 Fixation/Permeabilization Concentrate and Diluent kit, followed by staining with fluorophore-labeled anti-active Caspase-3 antibodies for 60 min on ice. For analyzing purified human or mouse CD8 T cells, cells with different treatments were first incubated with anti-CD16/CD32 antibodies for 10 min, and then stained with a fixable Aqua viability dye and a cocktail of antibodies for the surface markers for 30 min on ice. Cells were then fixed and permeabilized with the FOXP3 Fixation/Permeabilization Concentrate and Diluent kit, and subsequently stained for intracellular markers for 60 min on ice. For analyzing tumor-infiltrating, splenic or lymph node T cells from mice, the tumor, spleen and lymph node samples were harvested for preparation of single cell suspensions. Red blood cells were lysed using ACK lysis buffer. Single cell suspensions were then incubated with anti-CD16/CD32 antibodies for 10 min, and then stained with a cocktail of antibodies for the surface markers for 30 min on ice. After that, cells were fixed and permeabilized, and subsequently stained for intracellular markers for 60 minutes on ice.
Instrument	LSR II cytometer (BD Biosciences)
Software	FACSDiva software (BD Biosciences) was used to collect events on the LSR II, and FlowJo software (TreeStar) was used to analyze the data.
Cell population abundance	N/A
Gating strategy	Single cell gates based on FSC-H and FSC-A, and SSC-H and SSC-A were used to exclude non-singlets. A morphology gate based on FSC-A and SSC-A was used to exclude debrees. A live/dead cell gate based on fixable viability dye was used to exclude dead cells. For analyzing the positivity of cleaved-Caspase-3 in cells, cells stained with isotype control antibodies were used to define the background non-specific staining, and then a cleaved-Caspase-3+ gate was used for cells stained with cleaved-Caspase-3

specific antibodies based on the background. For identifying CD8 T cells, a CD3+CD8+CD4- gating strategy was used. For analyzing the PD-1 expression and activation status of CD8 T cells, CD3+CD8+CD4- cells were gated for PD-1, Ki-67 and GzmB. For analyzing CD8 T cell proliferation using the CFSE dilution assay, divided cells showing diluted CFSE were gated by taking unstimulated CFSE-labeled cells and non-labeled cells as the controls, which showed the CFSE intensity of non-divided cells and auto-fluorescence of the cells, respectively.

☒ Tick this box to confirm that a figure exemplifying the gating strategy is provided in the Supplementary Information.